Diamagnetic Interactions in Superheated-Superconducting Microgranules under an External Magnetic Field

A. Peñaranda[1] , C.E. Auguet[1], L. Ramírez-Piscina*[1] and TA. Girard[2]

1*Department de Física Aplicada,*

Universitat Politècnica de Catalunya,

Avda. Gregorio Marañon 44, E-08028 Barcelona, SPAIN.

2 *Centro de Física Nuclear,*

Universidade de Lisboa,

Av. Prof. Gama Pinto, 2, 1649-003 Lisbon, PORTUGAL.

(December 4, 2001)

ABSTRACT

The study of the phase transitions produced in ensembles of metastable superconducting granules by magnetic field variations holds interest for fundamental physics and for applications in particle detectors. It is a problem whose theoretical study has been long hampered by the difficulty in treating diamagnetic interactions between granules. In this review we describe the behaviour of such systems, develop the numerical procedures to deal with them, and present some experimental and numerical results.

KEYWORDS: Diamagnetic interactions, superconducting detectors, phase transitions.

---

*Author for correspondence: L. Ramírez-Piscina, Tel:34 934017995. Fax: 34 934017700. Email: laure@fa.upc.es

RESUM

L'estudi de les transicions produïdes en conjunts de grànuls superconductors metaestables té interès tant per la física fonamental com per aplicacions tals com detectors de partícules. L'estudi teòric d'aquest problema ha sigut obstaculitzat per la dificultat del tractament de les interaccions diamagnètiques entre grànuls. En aquesta revisió describim el comportament d'aquests sistemes, desarrollem el mètode numèric de tractament, i presentem alguns resultats experimentals i numèrics.

I. INTRODUCTION

Magnetic properties of ensembles of superconducting granules immersed in an external magnetic field have been a subject of long-standing interest in both basic and applied condensed matter physics. Historically, measurement of the supercritical fields of such suspensions has yielded determinations of the Ginzburg-Landau parameters [1], and have provided evidence for the nonlocal behaviour of Type I materials near the critical temperature. More recently, the superheated-to-normal phase transitions of Type I suspensions, induced by irradiation, have served as the basis for the development of particle detectors in a variety of areas, such as dark matter [2,3], neutrino [4], neutron [5], x-ray [6] and transition radiation [7] detection.

The response of a superconducting grain depends on its location within the (T, H) phase space, as shown in Fig. 1. This location is different for each microgranule of a dispersion due to size distribution, surface defects, and mainly to the diamagnetic interactions between microgranules. These effects yield a typical 20% spread of the transition fields of the ensemble. The uncertainty in the minimum energy necessary for the transition generates difficulty in interpreting the results of device response [8,9].

In order to decrease this spread, ordered arrays of spherical indium grains produced from thin films deposited on mylar foils using photolithography techniques have been explored

[10]. Such PASS (Planar Arrays of Superconducting Spheres) devices [11] have yielded differential superheating curves in which the field spread is reduced by an order of magnitude. A PASS device was recently used to provide information on the Leggett "baked Alaska" mechanism, relevant to the formation of topological defects in cosmological phase transitions [12].

An important point, often neglected in the response analysis of either the disordered or ordered ensembles, whether they have been irradiated or not, is that the local surface magnetic field on each sphere is not constant, but changes after transitions of other spheres due to diamagnetic interactions. It is clear that to understand basic device response, it is necessary to know the variation of the local magnetic field at the surface of the superconducting granules in the presence of the ensemble-modified external field.

Calculations involving magnetostatic interactions between many bodies are not trivial. The first theoretical analyses of this problem treated the dielectric interactions between spheres within a dipolar and two-body approximation [13,14] and hence with a validity limited to very low densities. The most systematic effort in the theoretical interpretation of experiments has so far been the perturbative analyses of Geigenmüller [15,16], which yielded results on the successive transitions of the spheres when the magnetic field is increased from zero. In the regime of dilute suspensions, Geigenmüller [15] constructed a perturbative theory which calculated statistics of local surface fields on the granules and of the transitions induced by the external field. This theory is formally based on a cluster expansion, in such a way that all the quantities are expanded in powers of the volume fraction ρ occupied by the microgranules. In practice, the expansion is performed up to first order, which means that only two-body interactions are considered [15].

In this paper we review some recent advances in the interpretations of experiments involving superconducting granules. In the next section we describe the essential ingredients of the phase space behaviour of a grain ensemble, using a "hot border" model developed for particle detection [17]. In the following section we detail our numerical method for calculating local surface fields [18]. This method solves the complete Laplace equation

for the magnetic field in the presence of a large number of superconducting granules. The maximum field values on the granules surfaces can be worked out, which enables simulations of granule transitions to be performed. In subsequent sections, we present numerical results for two typical experimental configurations. The first, which we refer to as "disordered", corresponds to the spheres being homogeneously diluted in a dielectric wax [19]. The second configuration, which we call "regular", corresponds to the PASS structure [11]. In each section, we provide results on both the maximum magnetic field on the surfaces of the microspheres, and on the successive transitions which occur when the external field is slowly increased from zero [20]. We obtain quantitative results of the surface magnetic field on the superconducting spheres during these transitions. We also compare simulation results in the disordered case with those obtained from the perturbative theory [21]. The last section is devoted to conclusions.

II. THE ENSEMBLE PHASE SPACE

The behaviour of each superconducting grain in an applied magnetic field, H_a, depends on its location in (T, H) phase space. In Fig. 2, we show the state of a generic grain ensemble at fixed temperature below T_c [17]. For a particular configuration of granule positions, surface defects and grain sizes, the distribution of maximum fields at the equator of each of the grains can be represented by the vertical line xy. With regard to granules in the superconducting state, those with a greater number of defects are generally located nearer the transition line, and hence will transit earlier under a H_a increase; the grains with lower values in the field distribution are those which are more metallurgically perfect.

For a given H_a some fraction of the suspension has transited to the normal state; each of the remaining grains sees a different maximum local field, H_l, resulting in a distribution $\Delta T = [T_{sh}(H_l) \Leftrightarrow T_a]$ required for transitions to the normal state, where $T_{sh}(H_l)$ is the superheated critical temperature for H_l. With an increase of H_a, an increasing fraction of the distribution transits to the normal phase. The loss of a part of the superconducting

population alters the field distribution of the remaining superconductors, in general reducing all local fields. Near the end of the field increase, the superconducting population is severely reduced and the diamagnetic effects are smaller; the last grain to transit is effectively a single grain transition without diamagnetic interactions, and represents the fundamental superconducting response of the material to magnetic fields. Measurements performed in this fashion enable determinations of the maximum superheating field H_{sh}, which is related to the Ginzburg-Landau parameter κ by

$$\kappa = \left[h_{sh}^2\sqrt{2}\right]^{-1} \tag{2.1}$$

where h_{sh}=H_{sh}/H_c.

Detector applications are based on the heating of a grain by the energy deposited by incident radiation which, depending on the grain location within the phase space, is either sufficient to raise the temperature ΔT across the phase line or is not. In principle, the maximum ΔE_{max} is able to induce the transitions of all grains within the region $\Delta H_{max} = H_{sh}(Ta) \Leftrightarrow H_\rho$ for which $\Delta T \leq \Delta T_{max} \sim C_p^{-1}\Delta E_{max}$.

For sufficiently long irradiation times or intense radiation fields, all of the grains within this region should become normal. The presence of the radiation field should thus create a quasi-phase boundary at H_ρ, which is determined by the maximum energy loss of the incident radiation and C_p. This "hot border" is not a conventional phase boundary: a grain transiting this border is turned to the normal state only by thermal nucleation; no magnetic nucleation is possible until the highest local field has achieved the usual superheated-normal transition value.

For a subsequent increase of H_a by δH, where $H_{sh} \Leftrightarrow H_\rho < H_a + \delta H < H_{sh}$, the maximum local fields of all grains that are still superconducting are similarly increased, in effect shifting xy upwards across the hot border by δH so that grains in the region $H_\rho \Leftrightarrow \delta H$ spread into ΔH_{max}. However, these can transite to the normal state only as a result of temperature changes induced by the corresponding higher portion of the energy loss distribution, at a rate dependent upon the radiation flux and interaction cross-section. By sequentially increasing

δH, xy is increasingly shifted upwards so that an increasingly greater fraction of the grains below H_ρ are spread into this region; an increasingly smaller amount of energy deposition is required to heat them into the normal state. The number of grains which transite for each δH is proportional to the corresponding energy loss by the incident radiation, and therefore to the incident radiation that undergoes this energy loss.

As originally set up, this model subsumes any consideration of grain size within the distribution of local magnetic field states since it has been shown that with the absence of size effects at low temperatures, transition fields and grain size are effectively uncorrelated [17]. Since the distribution of magnetic field states is independent of size, each field state may be considered as populated by a distribution of grain sizes.

What is not size-independent is the heating of the grain induced by the energy deposition of the incident radiation, which in a global heating model is given, in general, by

$$\frac{\Delta E}{V} = \int_T^{T+\Delta T} C_s dT \tag{2.2}$$

where V is the grain volume. For the same deposition energy, smaller grains are heated up more; larger grains may however absorb more energy. Following irradiation, each state will be depopulated according to a ΔE_{max} for which V yields a ΔT greater than that required for the phase transition, which does not, however guarantee that, following a sufficiently long time, a given magnetic state will be completely depopulated.

Eq. (2.2) in effect implies the existence of a $\Delta T_{max} \Leftrightarrow \Delta E_{max}/V_{min}$ with V_{min} the minimum grain size of the suspension, and ΔE_{max} the maximum energy deposited into V_{min}. All grains of size V_{min} lying near the phase line will transit under this energy deposition; larger grains will not, since ΔT will be insufficient to reach the phase line. This of course implies the existence of a $\Delta T_{min} \Leftrightarrow \Delta E'_{max}/V_{max}$ where $E'_{max} \neq \Delta E_{max}$ in general, since $\Delta E = \Delta E(V)$. This represents the minimum temperature increase of a suspension grain provoked by the irradiation. Following a sufficiently large $\Delta E'_{max}$ and long irradiation, the true "hot border zone", i.e. the region in which no superconducting grains exist, should lie only $\Delta H_{min} \Leftrightarrow \Delta T_{min}$ below the phase line [22]. Between ΔH_{min} and ΔH_{max}, the

superconducting grain population is only partially depleted and it is ordered according to decreasing size as distance increases from the phase line. An increase of the applied field after a pause, but in the absence of radiation, should yield no transitions until $H_{pause} + \Delta H_{min}$, and the irradiated-non-irradiated differential superheating curves should again be identical at $H_{pause} + \Delta H_{max}$.

III. NUMERICAL METHOD

It is now clear that for a proper interpretation of experiments involving transitions of superconducting granules, information on the distribution of local magnetic fields on the granules surface is needed. In this section we describe the numerical method employed to calculate these surface fields taking the complete diamagnetic interactions between granules into account. Let us consider a dispersion of N superconducting spheres placed at given positions $\mathbf{R}_i$ according to the desired geometry. We consider that all the spheres have the same radius, a, much greater than the London penetration length, and that the transitions of each to the normal phase is considered to be complete when the local magnetic field at any point on its surface reaches a threshold value B_{th}. Hence, we do not consider partial transitions to the intermediate state. Finally, it is assumed that the spheres remain at constant temperature, that is, we neglect the latent heat released by the microspheres when they transite.

The magnetic field $\mathbf{B}(\mathbf{r})$ is determined from a scalar potential $U(\mathbf{r})$

$$\mathbf{B}(\mathbf{r}) = \Leftrightarrow \nabla U(\mathbf{r}), \tag{3.1}$$

which satisfies the Laplace equation

$$\nabla^2 U(\mathbf{r}) = 0. \tag{3.2}$$

Two boundary conditions must be imposed. Firstly, for any superconducting sphere the magnetic field is tangent to the surface, *i.e.* the normal derivative of the potential vanishes. Secondly, the value of the field very far from the sample should match $\mathbf{B}_{ext}$:

$$U(\mathbf{r}) \to -\mathbf{r} \cdot \mathbf{B}_{ext} \ \ (r \to \infty). \tag{3.3}$$

The scalar potential $U(\mathbf{R}_j + \mathbf{r}_j)$ near sphere j can be expanded in multipoles [15,16] which, introducing the boundary conditions at the surface of the sphere, can be written as

$$U(\mathbf{R}_j + \mathbf{r}_j) = \sum_{\lambda=1}^{\infty} \sum_{\mu=-\lambda}^{\lambda} Y_{\lambda\mu}(\hat{r}_j) \; c_{\lambda\mu}(j) \left\{ \left(\frac{a}{r_j} \right)^{\lambda+1} + \frac{\lambda+1}{\lambda} \left(\frac{r_j}{a} \right)^{\lambda} \right\} + K(j), \tag{3.4}$$

where $Y_{\lambda\mu}(\hat{r}_j)$ are spherical harmonics, and $c_{\lambda\mu}(j)$ and $K(j)$ are the coefficients of the expansion. There is one of these expansions for each sphere. After determining the values of the unknown $c_{\lambda\mu}(j)$ and $K(j)$ for a given configuration, it is possible to calculate the surface fields from Eq. (3.4). The aim is to do this by cutting these expansions at some appropriate multipolar order, according to the required precision.

Taking all the expansions together with the boundary conditions, the coefficients satisfy the following equations [16]:

$$K(j) = -\mathbf{R}_j \cdot \mathbf{B}_{ext} + \sum_{k \neq j} \sum_{\lambda=1}^{\infty} \sum_{\mu=-\lambda}^{\lambda} A_{00\,\lambda\mu}(j,k) \; c_{\lambda\mu}(k) \tag{3.5}$$

$$\frac{\lambda+1}{\lambda} \; c_{\lambda\mu}(j) = -\sqrt{\frac{4\pi}{3}} B_{ext} \; a \; \delta_{\lambda 1} \delta_{\mu 0} + \sum_{k \neq j} \sum_{\lambda'=1}^{\infty} \sum_{\mu'=-\lambda'}^{\lambda'} A_{\lambda\mu\,\lambda'\mu'}(j,k) \; c_{\lambda'\mu'}(k) \tag{3.6}$$

where the constants $A_{\lambda\mu\,\lambda'\mu'}(j,k)$ are given in Ref. [18]. In Eq. (3.6) we have placed the external field in the z-direction.

The constants $K(j)$ only give additive contributions to the potential and do not affect the magnetic field values, so the problem is, in principle, to solve the (very large) set of linear equations (3.6) for the unknown c.

To directly find the values of the coefficients c for a given configuration with a representative number N of spheres turns out to be impractical. We therefore develop the following iterative method [18]. Eq. (3.6) can formally be written as a matrix equation for the vector of unknown $\mathbf{c}$

$$\mathbf{c} = \mathbf{b} + A\mathbf{c} \tag{3.7}$$

whose solution is

$$\mathbf{c} = (I \Leftrightarrow A)^{-1}\mathbf{b} \tag{3.8}$$

which can be expanded as a power series in A,

$$\mathbf{c} = \left(I + A + A^2 + A^3 + ...\right)\mathbf{b}. \tag{3.9}$$

One practical way to numerically perform this expansion is to apply the iteration

$$\mathbf{c}_{i+1} = \mathbf{b} + A\mathbf{c}_i, \tag{3.10}$$

$$\mathbf{c}_0 = \mathbf{b}. \tag{3.11}$$

It can be shown that this expansion is convergent as long as spheres do not touch each other, and the greater the distance between spheres, the faster the convergence. The desired precision is achieved by applying Eq. (3.10) iteratively until the change of the c coefficients is lower than a prescribed value.

Using the preceding numerical method we have calculated the local magnetic field on the surface of the spheres and, by standard minimization routines, the maximum magnetic surface field on each of the spheres. This information can then be employed in the interpretation of experimental results, for example, within the framework of the 'hot border' model above, or for performing simulations of relevant situations. Examples of such simulations will be presented in the following sections.

IV. DISORDERED DISTRIBUTIONS OF GRANULES

In this section we present numerical results corresponding to the ensemble of spatially disordered configurations of spheres. Experimentally this corresponds to configurations obtained by immersing the granules in paraffin wax and through a repeated number of baker's transformations [19].

A. Static Field Response

We consider samples of size $L \times L \times 0.1L$, immersed in an external magnetic field applied in the direction normal to the sample. The value of L is given by the fraction ρ of volume occupied by the spheres (the filling factor) and by the number of granules N in the dispersion. We have simulated samples with values of $\rho = 0.01$, 0.025, 0.05, 0.10, 0.15 and 0.20. Considering the number of granules, and due to the large order of the interactions, one should work with systems that are as large as possible, and perform some kind of extrapolation to infinite-sized system (experiments are indeed performed using values of N that are much larger than what is feasible by simulation techniques).

The effect of the dependence of the results on N is shown in Fig. 3, where typical distributions of maximum surface fields for the cases of $\rho = 0.01$ and 0.20 are presented for systems with different number of spheres. In the most dilute case (Fig. 3.a) it can be seen that the distribution is very narrow, with a high fraction of spheres having values of B_{max} very close to the value corresponding to an isolated sphere $\frac{3}{2}B_{ext}$. The highest maximum fields correspond to spheres in close proximity, with an inter-sphere gap of order 0.1 times the radius, which generates strong local fields. In the more concentrated case (Fig. 3.b) diamagnetic interactions are more important, so the maximum fields take on much larger values. The broadening of the field distributions induced by disorder appears to increase with N, associated with a tendency to reach greater maximum field values.

An analysis of the statistical properties of these distributions reveals a strong dependence of the mean field values on N for the largest filling factor, and only an extrapolation for $1/N \to 0$ would, in principle, permit a result for an infinite system. For the larger ρ, the variances of standard deviation are larger, fluctuating around a roughly constant value. The results of higher distribution moments, skewness and kurtosis, surprisingly show a stronger dependence on N for dilute systems. For the smaller ρ, the variability of these quantities is larger than in the most dense system. In particular, the kurtosis presents a clear increase with N, and we cannot exclude the possibility of a divergent value for an infinite system.

However, for the largest filling factor these values are nearly constant and very close to zero, *i.e.* the distribution seems to be more Gaussian.

The effect of spheres concentration is shown in Fig. 4, where we present the distribution of maximum surface fields for several values of the filling factor, and for the greatest N employed in each case ($N = 100$ for smaller ρ and $N = 150$ for $\rho = 0.15$ and 0.20). The distribution for the most diluted case is peaked near the isolated sphere value $\frac{3}{2}B_{ex}$, and tends to broaden and shift to higher field values as ρ increases. This can be due to the fact that there is a greater probability of finding close spheres when ρ increases, with the consequent increase of diamagnetic interactions. These effects are more clearly shown in Fig. 5, where we plot the mean value and the standard deviation of B_{max}. In order to estimate the statistical uncertainty, we have employed two independent configurations for each $\rho = 0.01$, 0.15 and 0.20. Both the mean of B_{max} and the standard deviation presents a fairly linear behaviour in ρ over the range of filling factors employed in the simulations.

In Fig. 6 the values of the skewness and the kurtosis of the distribution are represented as functions of ρ. Both quantities show a rapid decay to small values as ρ reaches values of the order of 0.1. In particular, the kurtosis is very close to zero and the skewness only slightly greater, with a very small statistical uncertainty. We therefore conclude that for such dense systems the distributions of maximum surface fields are clearly Gaussian. It is worthwhile noting the large statistical variability observed in the kurtosis for the least dense case.

B. Increasing Field Behaviour

Knowledge of the maximum local surface field of each sphere allows us to study transitions produced in the ensemble. We will consider here transitions induced by an increase of the external magnetic field, but one could, in principle, consider also radiation-induced transitions. An interesting feature of performing direct numerical simulations is that one can monitor quantities such as these local fields during transitions, which is information that

is not experimentally accessible.

In the calculus, we assume that the granules remain superconducting until their local surface fields reach a threshold value B_{th}, for which the spheres are completely in the normal state. The threshold value for a sphere free of defects would be the superheating field value B_{SH}. In order to take into account the possibility of defects, which can act as nucleation centres, we have employed a distribution of B_{th} values that was consistent with experiments for tin microspheres dispersed in paraffin [23]. This distribution was fitted by a parabolic distribution in a range of values between $0.8B_{SH}$ and B_{SH} [15,16]. As mentioned above, we consider that the sample is maintained at constant temperature and in our calculations the latent heat released in the transitions is neglected.

The procedure in our simulations is thus as follows: N superconducting spheres are placed at random according to the desired geometry and filling factor. The threshold value B_{th} for each sphere is also assigned by using the aforementioned distribution. Applying the iterative method described above, local values of the magnetic field and its maximum value on the surface of any sphere are determined. Comparison of these maximum surface fields with the respective values of B_{th} permits selection of the first superconducting sphere that will transit to the normal phase under an increase of the applied magnetic field. Furthermore, the precise value of B_{ext} at which the transition occurs is calculated. Subsequently, the system becomes one of $N \Leftrightarrow 1$ superconducting spheres. The long-range nature of the diamagnetic interactions changes the surface magnetic field values of the remaining superconducting spheres on any transition. This leads us to repeat the same calculation process after each transition until all spheres have transited. The transitions affect the volume occupied by the spheres that remain superconducting, and an effective filling factor ρ_{ef}, lower than the initial ρ value, can be defined.

Results shown in this section correspond to simulations on systems with a number of initially superconducting spheres $N = 250$ for dilute dispersions with ρ values from 0.001 up to 0.05, and $N = 150$ for denser systems with ρ up to 0.20. For each case we performed averages over a number of independent configurations between 2 to 7. The field-induced

transitions are presented in Fig. 7. In this figure the fraction f of remaining superconducting spheres during an increase of the external field versus B_{ext} is shown for different values of the initial filling factor ρ. The continuous line furthest to the right in this figure shows the expected behaviour for isolated spheres, for which the maximum surface field is equal to $3/2B_{ext}$, and therefore can be directly related to the distribution of B_{th} values. From the results of our simulations, represented by symbols in the figure, we observe that the transitions are produced for external field values very close to the threshold distribution values for the more dilute systems, except for a few transitions occurring at lower B_{ext} than expected. These transitions correspond to spheres whose distances to their nearest neighbour are not very large (about $0.10 \Leftrightarrow 0.15$ times the radius value). Therefore, for such a dilute case, the observed spread in the transition field values can be mainly attributed to surface defects. In the same figure we can observe that transitions appear for lower external fields as the concentration increases, and consequently the interval of external fields for which the transitions occur broadens. This effect is produced by diamagnetic interaction between the spheres, whose contribution to the local surface magnetic field becomes more important as the system becomes denser. We see that diamagnetic interactions begin to be the most important factor in transition spreading for filling factors of a few percent. Indeed, half of the spheres have undergone transitions at $B_{ext} = 0.48B_{sh}$ for $\rho = 0.20$, while for $\rho = 0.001$ a field $B_{ext} = 0.60B_{sh}$ is required.

Similar behaviour is observed experimentally. In Fig. 8, we show results reported by Dubos et. al. [24] and by Larrea *et. al.* [25]. The first set was obtained from a suspension of tin grains with diameters of $20 \Leftrightarrow 30$ microns with a volume filling factor of 20%. In contrast, the results of Larrea et. al. were obtained from measurements on suspensions of Sn microspheres, of diameter $33 \Leftrightarrow 40$ microns with volume filling factors of 4% and 25%. As seen in Fig. 8, half of the spheres transited at $B_{ext} = 0.48B_{sh}$ for $\rho = 0.25$, at $B_{ext} = 0.50B_{sh}$ for $\rho = 0.20$, and at $B_{ext} = 0.53B_{sh}$ for $\rho = 0.04$. This agreement confirms that the mechanisms involved in the simulations (presence of surface defects and influence of diamagnetic interactions) are essentially correct.

The stronger diamagnetic interactions correspond to the nearest spheres, so these will transit first. This fact modifies the spatial distribution in such a way that, after successive transitions, the remaining superconducting microgranules are further away, and present a certain spatial order. This is shown in Fig. 9 where we compare two configurations. In the first we see the $N = 25$ spheres that remain superconducting after transitions due to the increase of the external magnetic field over a system with initially $N = 150$ superconducting spheres placed at random, corresponding to $\rho = 0.20$. In the other, we see the spatial distribution of $N = 25$ spheres placed at random in the same volume.

On the other hand, the spatial order induced by an increasing external field will be reflected in the maximum surface magnetic field distributions, which is essential in analysing transitions. In Fig. 10 the results of our simulations for the distributions of maximum surface magnetic fields are represented by symbols for a configuration with initial $\rho = 0.20$ and for different values of external applied field, for which after successive transitions the configurations reach different values of ρ_{ef}. We observe that the width of the distributions decreases and consequently the maximum surface field values become more similar as B_{ext} (and hence the number of transitions) increase. This reveals the transitions as a strong ordering mechanism both in the spatial sense and in the surface magnetic distribution. This behaviour is also reflected experimentally in Fig. 8, where the $\rho = 0.20 \Leftrightarrow 0.25$ results converge to those of $\rho = 0.04$.

Statistical properties of surface field distributions are shown in Fig. 11. In this figure their mean values and standard deviations are represented versus the effective filling factor ρ_{ef}. We can observe that the maximum surface field approaches the isolated-sphere value $3/2B_{ext}$ as B_{ext} increases (ρ_{ef} decreases), and the standard deviation tends to zero, indicating an increase of the uniformity of the system. This confirms the homogenizing effect produced by transitions. In the inset on the same figure, skewness and kurtosis of distributions are shown in function of ρ_{ef}. Values of kurtosis, which are very close to zero for the dense random configuration, evolve to values very close to $\Leftrightarrow 1$ after several transitions. Therefore, the distribution of fields is much flatter than the Gaussian distribution. On

the other hand, skewness values drop to zero with transitions, *i.e.* random configurations present a strongly asymmetrical field distribution that evolve to a symmetrical distribution for transited samples.

Our results agree in the geometrical aspect with what was presented in [13] for two-dimensional samples, but we have no evidence of the clustering effect for three-dimensional samples predicted in the same reference from mean-field calculations. This is probably due to our use of very thin samples (with a height-width ratio of 0.1) in simulations. As regards the maximum surface field distribution, the higher moments from our simulations present an asymmetrical distribution of maximum field values, which evolve to a non-Gaussian symmetrical distribution. However, results in Ref. [14] (for $\rho = 0.10$), where only two-body dipolar interactions were taken into account, showed a symmetrical Gaussian-like distribution that evolved to a strongly asymmetrical distribution. We can conclude that the complete calculation, which uses higher order multipolar and multibody contributions to the magnetic field, is an essential ingredient of this kind of simulations.

It is interesting to compare the evolution of several configurations with different initial ρ, which after a different number of transitions, reach the same final ρ_{ef}. In Fig. 12 the maximum surface field distributions for systems in which the remaining superconducting spheres correspond to the same final $\rho_{ef} = 0.02$ are shown. They are compared with a configuration corresponding to $\rho = 0.02$ with the granules placed at random without transitions. It can be seen that when these systems evolve towards the same ρ_{ef}, the order induced by the successive transitions produces a final situation with much smaller field spreading. This is more evident in configurations with higher initial ρ that have undergone a greater number of transitions. In the random configuration, the effect of disorder is reflected in the width of the distribution. The mean maximum field value and the standard deviation, in the inset of this figure, confirm the homogeneity of the transited systems compared with the random system.

In all these results, the tendency to regularity or homogeneity in magnetic fields can be interpreted as a consequence of the positional order induced by the successive transitions.

A measure of this order can be made by studying the distances between each sphere that is still superconducting to the nearest superconducting sphere. The mean value of this magnitude is represented in Fig. 13 for the same configurations as in Fig. 12, as a function of their initial ρ. In this figure, all the configurations have the same effective filling factor, but the distances between superconducting spheres increase strongly with the initial ρ, and consequently with the number of transitions.

C. Comparison with Perturbative Theory

The perturbative theory developed by Geigenmüller [15] is formally based on a cluster expansion that takes into account the diamagnetic interactions and the influence of defects. In this theory all the quantities are expanded in powers of the filling factor ρ occupied by the microgranules.

In the dilute regime, the perturbative theory was applied to calculate statistics of local surface fields on the granules and of the transitions induced by the external field. Within this framework the fraction of spheres that remain superconducting for an external magnetic field value, B_{ext}, can be written as:

$$f(B_{ext}, \rho) = f_0(B_{ext}) + \rho f_1(B_{ext}) + O(\rho^2) \tag{4.1}$$

where the zeroth order term corresponds to isolated spheres. Therefore, $f_0(B_{ext})$ corresponds exactly to the distribution of threshold fields B_{th} if we take into account the fact that the maximum surface field of an isolated sphere is $\frac{3}{2}\ B_{ext}$, *i.e.* the zeroth order is the same predicted $\rho = 0$ value represented in Fig. 7. One interesting consequence is that this expansion can be used to obtain the distribution of B_{th} from experimental data by performing measurements on samples of different densities and extrapolating the results to $\rho \to 0$ [15,16,23].

In the expansion 4.1, each order can be calculated from the distribution of threshold fields B_{th}, and involves increasingly higher order contributions both in the number of spheres and

in multipolar interactions. In the present state of the theory, calculations are performed up to first order, which is equivalent to considering only two-body interactions. The comparison between our simulations and the results of the Geigenmüller theory can give an idea of the contribution of multibody interactions and enables us to define the range of validity of the linear approximation, and it will also provide an insight into the effects of higher order terms.

To this end, Fig. 7 also shows the predictions of Eq. 4.1 and Ref. [15] for $\rho = 0$, 0.01, 0.05 and 0.10 as continuous lines. We see that the theory does contain the observed trend of transitions to occur for lower external fields due to diamagnetic interactions, but agreement does not seem to be quantitative except for extremely dilute samples. For the 5% case agreement appears to be rather poor and it is even worse for denser systems.

A more appropriate test of the linear approximation involved in Eq. 4.1 is the study of the dependence of f on the density ρ for different values of B_{ext}. This is shown in Fig. 14, where symbols represent simulation results and lines are the perturbative predictions of Eq. 4.1. Note that the evolution of a system during successive transitions is represented by points at constant ρ and increasing values of B_{ext}. We see that the perturbative calculation of Eq. 4.1 provides a correct qualitative picture of the transitions. However, for intermediate values of B_{ext}, the differences between theory and simulations start to become non-negligible at volume fractions between 2 - 5%. These results further indicate that $\rho \to 0$ extrapolations of experimental results, performed in order to obtain information on the distribution of values of B_{th}, should only be made with very dilute systems. This may explain the apparent discrepancies between theory and experiment found in Refs. [15,23], where the values of f_0 and f_1 were evaluated by linear extrapolations of experimental data up to $\rho = 5\%$. In view of Fig. 14, this procedure should yield erroneous results in the range of the most interesting values of B_{ext}, where transitions mostly occur. It is precisely in this range where the contribution of f_1 in Eq. 4.1 is more important, so it is here where a breakdown of the perturbative scheme is expected [15].

The theory of Geigenmüller also provides estimates of the distribution of values of such maximum fields in the small-density expansion [15]:

$$P(B_{max}, \rho) = P_0(B_{max}) + \rho P_1(B_{max}) + O(\rho^2) \tag{4.2}$$

In this equation $P(B_{max}, \rho)$ stands for the fraction of superconducting spheres with a maximum surface magnetic field smaller than B_{max}. We have omitted the implicit dependence of such quantities on B_{ext}. $P_0(B_{max})$ is the step function $\theta(B_{max} \Leftrightarrow 3/2B_{ext})$, *i.e.* the result for isolated spheres. The linear term describes the broadening of the distribution due to magnetic interactions [15]. These interactions change at each transition during the increase of the external field, and therefore are history dependent. This is the reason why the broadening described by P_1 depends on B_{ext}.

For dilute systems we have compared results of surface magnetic field distributions from our simulations with the theoretical calculus in dispersions with several values of ρ. Again, although the perturbative theory contains the qualitative behaviour, it only appears quantitatively correct for very small values of the occupied volume fraction. As in the case of the simulations, the evolution of a system under external field is analysed. The results obtained from the theory are represented by continuous lines in Fig. 10 for $\rho = 0.20$. We observe that the large discrepancies observed at $B_{ext} = 0.2B_{sh}$ evolve to a reasonable agreement for $B_{ext} = 0.5B_{sh}$ or $B_{ext} = 0.6B_{sh}$.

From the statistical results obtained by the perturbative theory, Fig. 11 shows that it predicts transitions only for external fields greater than $0.2B_{sh}$. We also see a similar qualitative behaviour between theory and simulation, but the quantitative results from the theory approach the simulation results quite satisfactorily for external fields greater than $0.4B_{sh}$ (or, in terms of fraction of volume of spheres that remain superconducting, $\rho_{ef} = 0.1$). This agreement between simulations and theory after transitions is quite surprising for such a dense case, and appears to be better than that obtained for low densities and low external fields. In order to check the effect of dilution produced by transitions, Fig. 10 also represents the distribution of maximum fields for a configuration with the same ρ_{ef} (slightly lower than 0.1) as that of $B_{ext} = 0.5B_{sh}$, but with positions completely at random, and the corresponding predictions from perturbative theory. Note the good agreement between

theory and simulations for the system which has been ordered by transitions compared with the discrepancies observed for the last random configuration with the same effective filling factor. We can conclude that the perturbative theory implicitly includes the homogenising effect of transitions. However this good behaviour of the theory is not completely explained by the decrease of the effective filling factor during the transition process.

V. ORDERED DISTRIBUTIONS OF SPHERES

In this section we present results from simulations of PASS systems, or ensembles of superconducting spheres placed in regular $2D$ square lattices of varible cell length d. The configurations studied correspond to planar arrays with B_{ext} normal to the plane, and do not correspond to a recent report of PASS response in a parallel field configuration [26]. Such regular configurations are not affected by disorder effects, but important finite-size effects can arise in this situation.

A. Static Field Response

The simulations were performed on systems with several concentrations (*i.e.* several lattice spacings) and different numbers of spheres up to $N = 169$. We have selected configurations with lattice spacing values $d/a = 7.482$, 4.376, 3.473, 3.034, and 2.757, which would correspond to tridimensional lattices for filling factors values 0.01, 0.05, 0.10, 0.15 and 0.20, in order to compare them with disordered configurations. The long range of diamagnetic interactions has led us to select the largest number of spheres possible, in particular for denser configurations, for which the finite size of systems will be more important.

The effect of the number of spheres considered in the study is shown in Fig. 15, where distributions of B_{max} are represented for several values of N and for filling factors $\rho = 0.01$, 0.1 and 0.2. For the most dilute case, the values of surface fields are nearly the same as on isolated spheres, and the effect of the number of spheres is not noticeable, as it corresponds to a spatial distribution where the spheres are very far away. However, when the concentration

of spheres is increased, the increment of diamagnetic interactions is very sensitive to the environment of each sphere. This is made clear in distributions for which an increment of N presents a clear increment in the surface magnetic fields. Spatial symmetry, with equivalent positions, is reflected in this distribution as a discontinuous appearance, more evident for denser systems, where for symmetry reasons only a few maximum values of the surface field are possible. The distributions are very asymmetrical, with a tendency for B_{max} to assume values close to the largest one, and with strong finite-size effects. We can explain these features by analysing what happens in a large system and comparing it to an infinite system. In an infinite planar lattice, all the field lines have to pass between the spheres, and all spheres have a high value of the maximum surface field. However, for a finite system most of the field lines can easily round the sample, and the surface fields turn out to be distinctly smaller than in the infinite system. This is a manifestation of the well-known fact that diamagnetic interactions are long range.

All these is clearly shown in results of statistical properties of the distributions. The mean values of B_{max} present important size effects. Low standard deviation values show that the system has a number of nearly equivalent positions, those far from the borders, whose proportion should increase with the size of the system. Indeed, for the largest systems the standard deviation decreases with the number of spheres. Skewness and kurtosis values are very different from zero, and their absolute values tend to increase with N. As in the most dilute disordered case, the kurtosis seems to diverge in the large N limit. The values of these moments present a non-Gaussian, very asymmetrical distribution.

The effect of different lattice spacing on the surface magnetic field distribution is presented in Fig. 16 for the largest systems simulated. The shape of these distributions is very different from the disordered shape, but does not show great qualitative changes with the increase of the filling factor. The field values and the distribution widths however show a strong increase with ρ. The reason is the aforementioned effect of finite size. In dilute configurations, the finite size of the system does not have a great influence on diamagnetic interaction, so the surface fields are very similar. As the lattice spacing decreases, this finite

size has a greater influence. The spheres in the middle of the system will have a large number of closer neighbours, and consequently the surface field will be enhanced. This magnitude will be lower for spheres near the boundary of the system. This can be seen in Fig. 17, where the surface field values are represented as a function of the granule position for $\rho = 0.1$ and 0.2. We observe that the boundary effects are more important at higher filling factors. On the other hand, for more dilute systems the values of maximum fields are more similar.

Fig. 18 shows the mean values of the maximum surface fields corresponding to the distributions represented in Fig. 16, and the maximum of each distribution as a function of the lattice spacing. The values tend to diverge for concentrated systems as in the disordered cases. We see similar behaviour of the standard deviation, which we represent in Fig. 19 for the same distributions.

The values of the higher moments of the distributions are shown in Fig. 20 for the largest systems as a function of the lattice spacing. Again, results for these quantities turn out to behave in an opposite fashion to those of the disordered configurations. In particular, both absolute values increase with concentration. Moreover, the kurtosis seems to diverge. We conclude that, for ordered configurations, the non-Gaussianess of the distribution of maximum fields is higher for more concentrated systems.

B. Increasing Field Behaviour

For studying transitions we follow the same procedure as in disordered suspensions. The effect of possible defects on the surface of spheres is included with the same threshold distribution values B_{th}. In order to discover the evolution of systems from successive transitions we monitor the maximum magnetic field on the surface of remaining superconductor in each transition. The configurations selected in this analysis correspond to plane arrays with distances (d) between the centre of spheres, in units of radius 'a' of $d/a = 7.482$, 4.376, 3.473, 3.034, 2.756 and 2.5. The number of spheres N considered is 169 except for the most dilute case, for which transitions were analysed for 144 microgranules.

Results from simulations are shown in Fig. 21, where the fraction of remaining superconducting spheres as a function of the external field value (in units of B_{SH}) is represented for several lattice distances. We observe that for dilute systems, transitions are produced for external field values closest to the threshold distribution, but the transitions begin for lower external field values as the distance between spheres is decreased. This is a consequence of diamagnetic interactions, which are stronger for closer spheres, and is analogous to the same effect observed in the disordered configurations. An interesting result from this figure is the breakdown of the continuous response of dilute systems when the concentration increases, with the appearance of a "plateau zone'. This effect is produced for a fraction of remaining superconducting spheres of about 0.25. In this zone there is a gap in the necessary increment of the external field to generate the following transition. The width of this gap increases as lattice spacing is lowered.

A similar "plateau zone" was observed by Esteve et. al. [27] in a previous study. They studied configurations with a large number of spheres (100×100), but for which only two-body interactions and short-range interactions were taken into account, and with an *ad hoc* choice of transition rules of a random nature. They showed a 'plateau zone' that changed with the distance between spheres, but that was always located around $f(B_{ext}) = 0.3$.

In order to analyse this effect, we studied the dynamics of the system in its evolution with an increase of the external field, both in the spatial configuration and in its distributions of surface field. Some of our results are represented in Fig. 22, which shows the maximum surface magnetic field distributions for a configuration with $d/a = 2.756$ for some external applied fields (always in B_{sh} units). We see that the transitions induced by the external field make the field distribution split into two branches with a gap or plateau between them. This discontinuity between both branches eventually disappears for a sufficiently high external field. By looking closely at the spatial position of the spheres, we observe that each branch corresponds to spheres that either have or have not superconducting next neighbours. When a microgranule transits, the surface field of the closest neighbours decreases as a consequence of diamagnetic interactions. Indeed, each time that a sphere transits the next neighbour

undergoes a significant loss of its local surface field, which is reflected in the figure as the switching of that sphere from one branch to the other. When the first branch disappears the system is in the "plateau zone" and not one of the spheres has a superconducting next neighbour. For high concentration and a great number of spheres, another "plateau zone" with a lower interval for the disappearance of second neighbours could be observed. This subject is presently under study.

The "plateau zone" has interesting consequences for PASS operation, since it corresponds to an effective "hot border" in the phase diagram, as described above. In the case of disordered configurations, the border is created by raising the magnetic field above H_{pause} by δH, then reducing H_a to H_{pause}. In this present case, the zone width is dictated by the plateau. As the field is slowly increased across the plateau, no magnetically-induced transitions occur; any transitions would correspond uniquely to irradiation-induced phase transitions.

There is at present no experimental evidence in support of either the existence of the plateau zone or its irradiation response. The majority of PASS experiments have been done with a fixed magnetic field under temperature variations [10]; the recent report of PASS behaviour by the Bern group, [26] while magnetically-driven, was obtained from arrays with effective concentrations that were too low to observe the plateau.

VI. CONCLUSIONS

In this review we have described numerical and experimental results involving systems of metastable supermagnetic granules. Transitions of such systems have relevance in both fundamental and applied studies in condensed matter physics. In particular we have addressed situations which are relevant to applications in particle detection.

A crucial point in the study of these systems is the calculation of the local magnetic field. The numerical method developed for our simulations allows us to reach the desired precision by considering multipolar and multi-body interactions. This method has been applied to

both disordered and ordered configurations of superheated superconducting microgranules. Disordered configurations correspond to experiments employing dispersions of granules diluted in a wax matrix. Ordered configurations correspond to the PASS experimental set-up.

We have obtained Gaussian-like behaviour of surface magnetic field distributions of disordered systems, especially for higher concentrations. On the other hand, the ordered configurations present non-Gaussian field distributions, principally for higher concentrations. Moreover, these ordered configurations show important finite size effects.

The possibility of calculating the maximum local surface field on each granule allows simulations of transitions to be performed. Results are presented for transitions produced by increases in the external applied field. We can obtain further information such as local fields on the granules that cannot be easily obtained in experiments. This would allow insight to be gained into the physics involved in the process, and to test models constructed to interpret experimental results.

Simulations of evolution of initially disordered configurations show that the configurations obtained after several transitions are much more ordered, in the sense that the positions of the remaining superconducting granules are not completely random. On the other hand, the spheres tend to keep apart from each other and, as a consequence, the local surface fields become more uniform in the system. This has important practical consequences in estimating and reducing uncertainties in Superheated Superconducting Granules experiments.

From the results on transitions in initially ordered systems, we observe that dense configurations present a discontinuity or 'plateau zone' as a consequence of spatial distribution evolution. This plateau corresponds to an effective 'hot border' with interesting consequences for PASS operations.

We have also compared our numerical results with the existing perturbative theory. The theory qualitatively predicts the transitions and the local field statistics. However, this theory is quantitatively correct only for very dilute samples, with occupied volume fractions of at most 1 - 2%. Therefore such expansions, although providing a very useful framework for analysing experimental results, should be used with caution in obtaining quantitative

information. In particular, extrapolation to the zero concentration limit of experimental data should only be performed for very dilute samples, within the validity range of the expansion. This range increases for systems initially at higher densities after having undergone a large number of transitions.

Direct simulations of SSG systems appear as a promising technique in analysing and complementing experimental results. In particular, diamagnetic interactions, which were only partially considered in previous studies, can be completely incorporated in simulations and appear to be an essential ingredient in the behaviour of such systems. The consideration of radiation-induced transitions, currently under study, should be of relevance in particle detection applications.

ACKNOWLEDGMENTS

We acknowledge financial support from Dirección General de Investigación Científica y Técnica (Spain) (Project BFM2000-0624-C03-02) and Comissionat per a Universitats i Recerca (Spain) (Projects 1999SGR00145 and 2000XT0005). We also acknowledge computing support from Fundació Catalana per a la Recerca-Centre de Supercomputació de Catalunya (Spain). TAG acknowledges financial support from Fundação para Ciencia e Tecnologia of Portugal under PRAXIS/FIS/10033/98.

REFERENCES

[1] Smith F.W., Baratoff A. and Cardona M.: "Superheating, Supercooling, Surface Superconductivity and Ginzburg-Landau Parameters of Pure Type-I Superconductors and Their Alloys", Phys. Kondens. Materie 12 (1970) 145.

[2] Casalbuoni S., Czapek G., Hasenbalg F., Hauser M., Janos S., Moser U., Pretzl K., Sahli B., van den Brandt B., Konter J.A., Mango S., Ebert T., Kainer K.U., and Knoop K.M.: "The ORPHEUS Dark Matter Experiment", in Proc. Carolina Symposium on Neutrino Physics, ed. Bahcall J., Haxton W., Kubodera K., and Poole C. (World Scientific, Singapore, 2001) 310.

[3] Girard T.A., Collar J.I., Waysand W. and Morales A.: "Status of the SALOPARD Experiment", in Proc. 1st Intl. Workshop on the Identification of Dark Matter, ed. Spooner N.J.C. (World Scientific, Singapore, 1997), p. 456.

[4] Girard T.A.: "Recent Progress in Metastable Superconducting Detectors and Possibilities for Neutrino Mass Searches", in Perspectives in Neutrinos, Atomic Physics and Gravitation, ed. Tran Thanh Van, Damour T., Hinds E. and Wilkerson J. (Editions Frontieres, Gif-sur-Yvette, 1993) 25.

[5] Meagher G., Pond J., Kotlicki A., Turrell B.G. and Drukier:A.K. "Neutron Detection using a Planar Array of Superheated Superconductors", Nucl. Instr. Meth. A370 (1995) 8.

[6] Heres O., Dubos H., Girard T.A., Limagne D., Perrier P., Torre J.P.and Waysand G.: "Response of a Metastable Superconducting Detector to 55Fe Irradiation Below 400 mK", Jour. Low Temp. Phys. 93 (1993) 449.

[7] Huang C.Y., Chen C.P., Yuan L.C.L., Lee S.C., Waysand G., Perrier P., Limagne D., Jeudy V. and Girard T.A.: "Study of a Novel Transition Radiation Detector Utilizing Superconducting Microspheres for Measuring the Energy of Relativistic High Energy

Charged Particles", Physica C341-348 (2000) 1963; Yuan L.C.L., Chen C.P., Huang C.Y., Lee S.C., Waysand G., Perrier P., Limagne D., Jeudy V. and Girard T.A."A Novel Transition Radiation Detector Utilizing Superconducting Microspheres for Measuring the Energy of Relativisitic High-Energy Charged Particles:", Nucl. Instr. Meth. A441 (2000) 479.

[8] Drukier A.K. and Vallete C., Nucl. Instrum. Methods 105 (1972) 285; Drukier A.K., Nucl. Instrum. Methods 173 (1980) 259, ibid 201 (1982) 77.

[9] Drukier A.K., Valette C., Waysand G., Yuan L.C.L. and Peters F., Lett. Nuovo Cimento 14 (1975) 300;

[10] Meagher G., Kotlicki A., He X.F., Eska G.and Turrell B.G.: "Planar Arrays of Superheated Superconductors", in Proc. "Superconductivity and Particle detection", ed. Girard T.A., Morales A. and Waysand G. (World Scientific, Singapore,1995) 147.

[11] Le Gros M., Da Silva A., Turrell B.G., KotlickiA. and Drukier A.K., Appl. Phys. Lett. 56 (1990) 2234.

[12] Meagher G., DiSanto D., Kotlicki A., Eska G. and Turrell B.G., "Nucleation of the supercooled Normal to superconducting phase transition in small Indium spheres induced by γ radiation", Phys. Rev. Lett. 79 No 2 (1997) 285-288.

[13] Valette C., Waysand G. and Stauffer D., "Diamagnetic interactions between superheated superconducting granules", Solid State Commun. 41 (1982) 305-307.

[14] Hillen M. and Stauffer D., "Monte Carlo simulation of three-dimensional suspensions of superconducting granules", Solid State Commun. 43, No. 6 (1982) 487-489.

[15] Geigenmüller U., "On dispersions of superheated superconducting spheres", J. Phys. (Paris) 49 (1988) 405-420.

[16] Geigenmüller U., "Magnetostatic interactions between superconducting spheres", in *Su-*

perconducting and Low-Temperature Particle Detectors, ed. Waysand G. and Chardin G., (Elsevier, 1989) 191-200.

[17] Waysand G., Girard T.A., Henriques R.P., Limagne D., CollarJ.I., Godinho M., Jeudy V., Pagesy V. and Bonfait G.: "A New Description of the Behavior of Metastable Superconducting Grains Suspensions Under Irradiation", J. Low Temp. Physics. 93 (1993) 485.

[18] Peñaranda A., Auguet C.E. and Ramírez-Piscina L., "Surface field in an ensemble of superconducting spheres under external magnetic field", Nucl. Instrum. and Meth. A424 (1999) 512-522.

[19] Jeudy V., Limagne D. and Waysand G., "On the reproducibility of the response of metastable superconducting detectors", Nucl. Phys. B (Proc. Suppl.) 28A (1992) 482-485.

[20] Peñaranda A., Auguet C.E. and Ramírez-Piscina L., "Transitions in disordered suspensions of superconducting granules under external magnetic field", Sol. State Comm. 109 No 4 (1999) 277-282.

[21] Peñaranda A., Auguet C.E. and Ramírez-Piscina L., "Diamagnetic interactions in disordered suspensions of metastable superconducting granules", unpublished work.

[22] Girard T.A.: "Irrradiation-induced Ordering of a Disordered Suspension of Superheated Microspheres", Nucl. Instr. Meth. A444 (2000) 353.

[23] Mettout B., Thesis, Université Paris VII, June 1988.

[24] Dubos H., Girard T.A., Waysand G., Perrier P., Jeudy V., Limagne D., Seco J. and Collar J.I.: "Thermal Nucleation of the Normal State in Superheated Superconducting Tin Grains", Phys. Rev. B58 (1998) 6468.

[25] Larrea A., Morales A., Waysand G. and Bartolomi J.: "Magnetic Properties in Tin

Superheated Superconducting Micrograin Suspensions: Test of Avalanche Effect", Nucl. Instr. Meth. A317 (1992) 541; Larrea A., Bartolomi J., Morales A., Morales J. and Waysand G.: "Magnetic Phase Diagram of Colloidal Superconducting Microspheres of Tin", J. Magn. and Mag,. Mat. 104-107 (1992) 229.

[26] Casalbuoni S., Czapek G., Hasenbalg F., Hauser M., Janos S., Pretzl K., Calatroni S., Sgobba S., and Vollenberg W.: "Phase Transition Study of Superheated Planar Arrays of Tin Cylinders", Nucl. Instr. Meth. A459 (2001) 469.

[27] Esteve J.G., Waysand G. and Laín S., "Analysis of the diamagnetic interactions of superheated-superconducting granules in a bidimensional array", Mechanics Research Comm., 27 No 1 (2000) 7-14.

FIGURES

FIG. 1. Phase diagram for a type I superconductor. ΔH and ΔT represent the increase of either the magnetic field or the temperature needed for a metastable superconductor grain at H_a, T_a to transit.

FIG. 2. Standard 'hot border' phase diagram.

FIG. 3. Fraction P of spheres with maximum surface field lower than the x-axes value (in units of B_{ext}) for disordered configurations with several values of N. (a) $\rho = 0.01$; (b) $\rho = 0.20$.

FIG. 4. Fraction P of spheres with maximum surface field lower than the x-axes value (in units of B_{ext}) for disordered configurations. $N = 100$ except for $\rho = 0.15$ and 0.20, for which $N = 150$.

FIG. 5. Mean value (circles) and standard deviation (squares) of the distribution of B_{max}/B_{ext} versus ρ (disordered configurations).

FIG. 6. Skewness (circles) and kurtosis (squares) of the distribution of B_{max}/B_{ext} versus ρ (disordered configurations).

FIG. 7. Fraction f of spheres that remain superconducting versus B_{ext}/B_{sh}, after an increase of the external magnetic field from zero, for different occupied volume fractions ρ. Symbols represent simulation results. From right to left, continuous lines correspond to predictions of Eq. 4.1 and Ref. [15] for $\rho = 0$, 0.01, 0.05 and 0.10. The case of $\rho = 0$ is the dilute limit, *i.e.* assuming a maximum surface field of $1.5B_{ext}$ for all the spheres.

FIG. 8. Experimental results of the fraction f of spheres that remain superconducting versus B_{ext}/B_c, after an increase of the external magnetic field from zero, for different occupied volume fractions ρ.

FIG. 9. Spatial distribution for $N = 25$ spheres: a) remaining superconducting after transitions from $N = 150$, b) placed at random.

FIG. 10. Fraction P of spheres with maximum surface field lower than the x-axis value (in units of B_{ext}), corresponding to an initial $\rho = 0.20$ for several values of external magnetic field. The results for a system with the same number of spheres that remain superconducting in the case of $B_{ext} = 0.5B_{sh}$, but placed at random are also represented. Continuous lines are the corresponding predictions of Eq. 4.2 and Ref. [15] The dashed line corresponds to the prediction for the random configuration.

FIG. 11. Mean value ($\circ$) and standard deviation ($\Box$) of the distribution of maximum surface field for evolution of a configuration with initially $\rho = 0.20$ and $N = 150$ as a function of ρ_{ef}. Results are averages of 5 independent samples. In the inset the corresponding skewness ($\triangle$) and kurtosis ($\diamond$) are shown for $\rho_{ef} \geq 0.10$ (statistical errors for these quantities are too large for smaller ρ_{ef}, owing to the small number of superconducting spheres involved). The results from the perturbative theory mean value ($*$) and standard deviation ($\times$) are represented.

FIG. 12. Fraction P of spheres with maximum surface field value lower than the x-axes value (in units of B_{ext}) for configurations with different initial ρ and the same final value $\rho_{ef} = 0.02$. In the inset the corresponding mean value ($\circ$) and standard deviation ($\Box$) as a function of ρ.

FIG. 13. Mean value of the distances between each sphere to its nearest neighbour, in units of the radius of the spheres a, for systems that evolve to the same final $\rho_{ef} = 0.02$, versus the initial ρ.

FIG. 14. Fraction f of spheres that remain superconducting in function of ρ for several values of B_{ext}. Symbols are simulation results: ($\circ$) $B_{ext} = 0.30B_{sh}$, ($\times$) $B_{ext} = 0.40B_{sh}$, ($\Box$) $B_{ext} = 0.50B_{sh}$, ($*$) $B_{ext} = 0.53B_{sh}$, ($\diamond$) $B_{ext} = 0.55B_{sh}$, ($+$) $B_{ext} = 0.58B_{sh}$, ($\triangle$) $B_{ext} = 0.60B_{sh}$, ($\bullet$) $B_{ext} = 0.62B_{sh}$, full squares $B_{ext} = 0.65B_{sh}$. From the top to the bottom, continuous lines are predictions of Eq. 4.1 and Ref. [15] for the same values of B_{ext}.

FIG. 15. Fraction P of spheres with maximum surface field lower than the x-axis value (in units of B_{ext}) for ordered configurations with several values of N. (a) $\rho = 0.01$; (b) $\rho = 0.10$; (c) $\rho = 0.20$.

FIG. 16. Fraction P of spheres with maximum surface field lower than the x-axes value (in units of B_{ext}) for ordered configurations. $N = 144$ except for $\rho = 0.10$ and 0.20, for which $N = 169$.

FIG. 17. Maximum surface field for spheres lying on a line crossing the square lattice in an ordered configuration. $N = 13 \times 13$.

FIG. 18. Mean value ($\circ$) and maximum value ($\Box$) of the distribution of B_{max}/B_{ext} versus the lattice spacing. In the inset the same quantities are represented versus ρ.

FIG. 19. Standard deviation of the distribution of B_{max}/B_{ext} versus the lattice spacing. In the inset the same quantities are represented versus ρ.

FIG. 20. Skewness ($\circ$) and kurtosis ($\Box$) of the distribution of B_{max}/B_{ext} versus the lattice spacing. In the inset the same quantities are represented versus ρ.

FIG. 21. Fraction f of still superconducting spheres versus B_{ext}/B_{sh}, after an increase of the external magnetic field from zero, for several samples of $N = 150$ initially superconducting spheres, corresponding to different initial lattice spacing. Continuous line corresponds to the dilute limit, *i.e.* assuming a maximum surface field of $3/2B_{ext}$ for all the spheres.

FIG. 22. Fraction P of spheres with maximum surface field lower than the x-axes value (in units of B_{ext}), in the evolution of a configuration with initially lattice spacing $d/a = 2.756$ ($\rho = 0.20$) and $N = 169$.

Fig. 1 Penaranda et al.

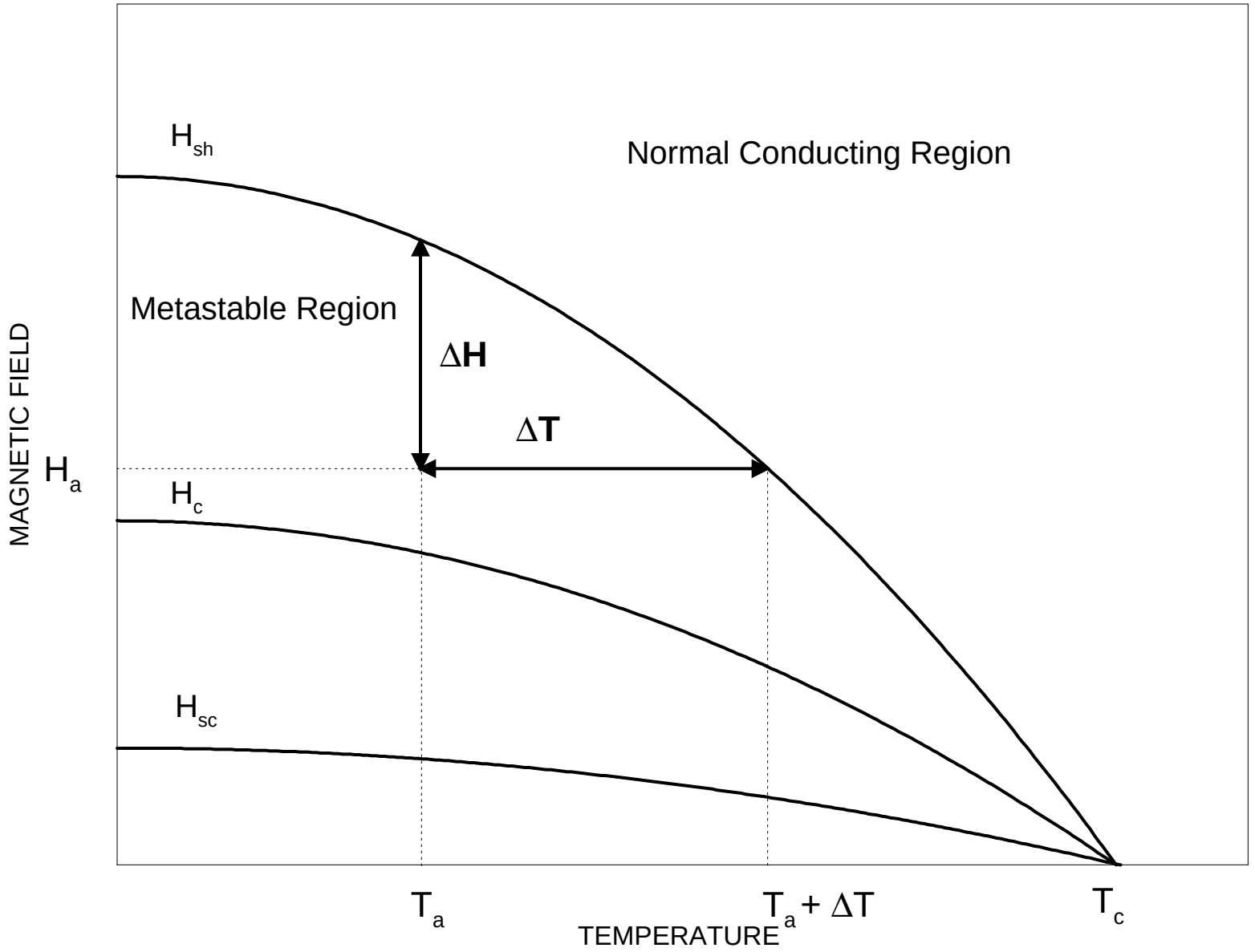

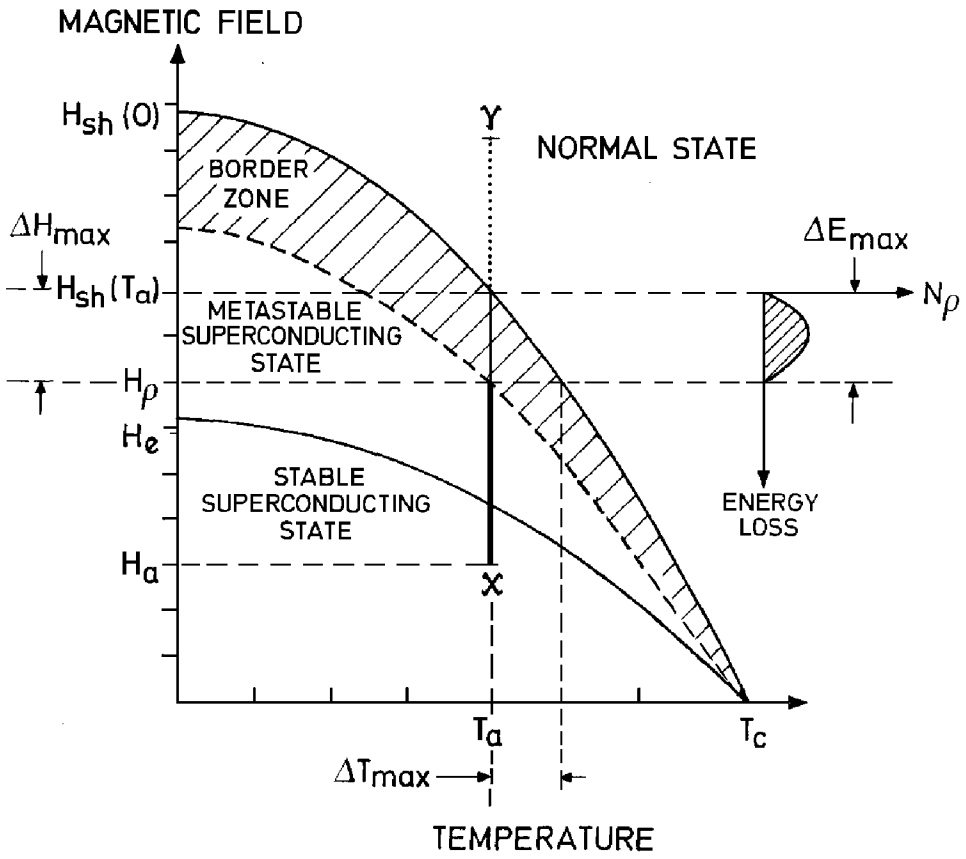

Figure 2 A. Penaranda et al.

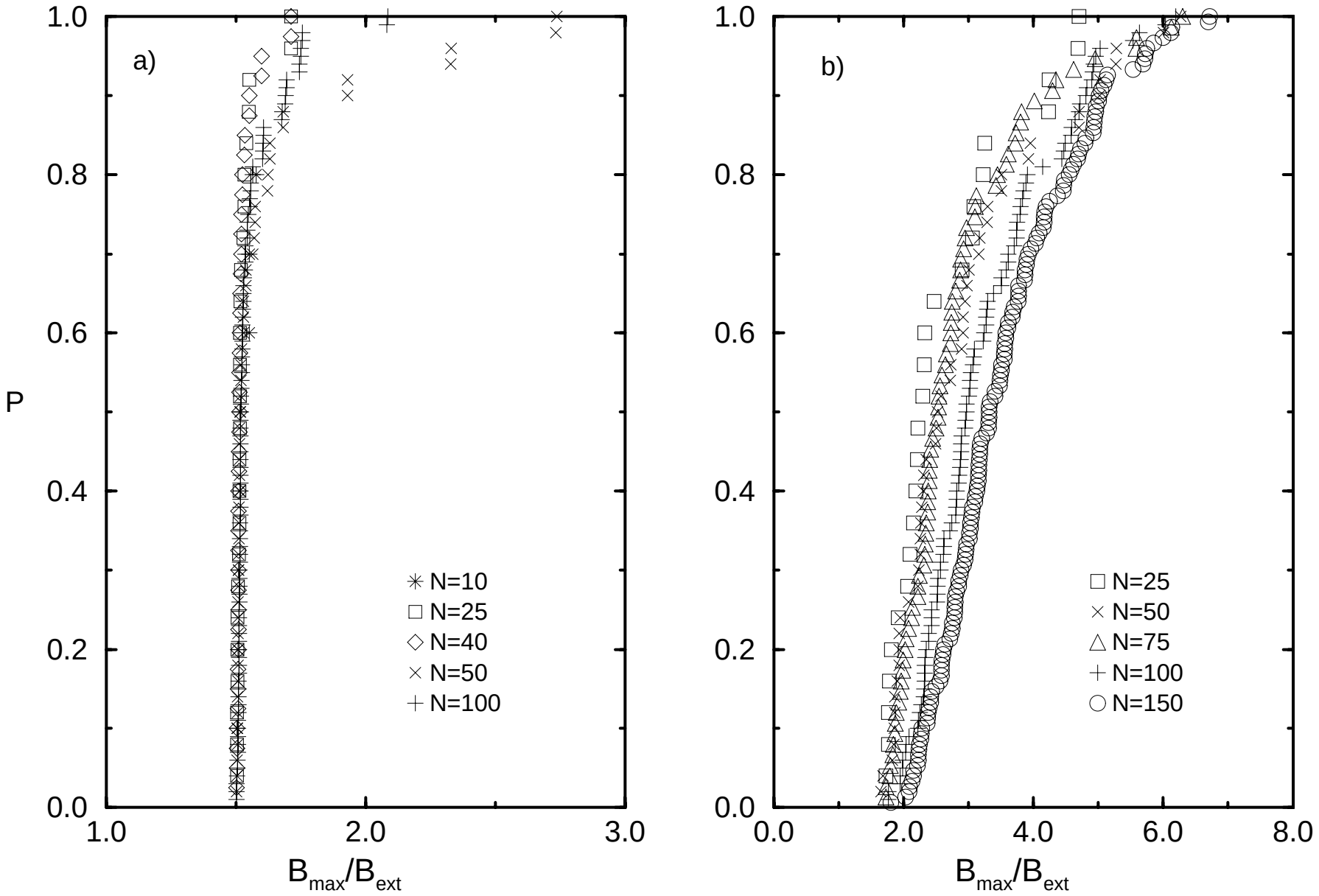

Fig. 3 A. Penaranda

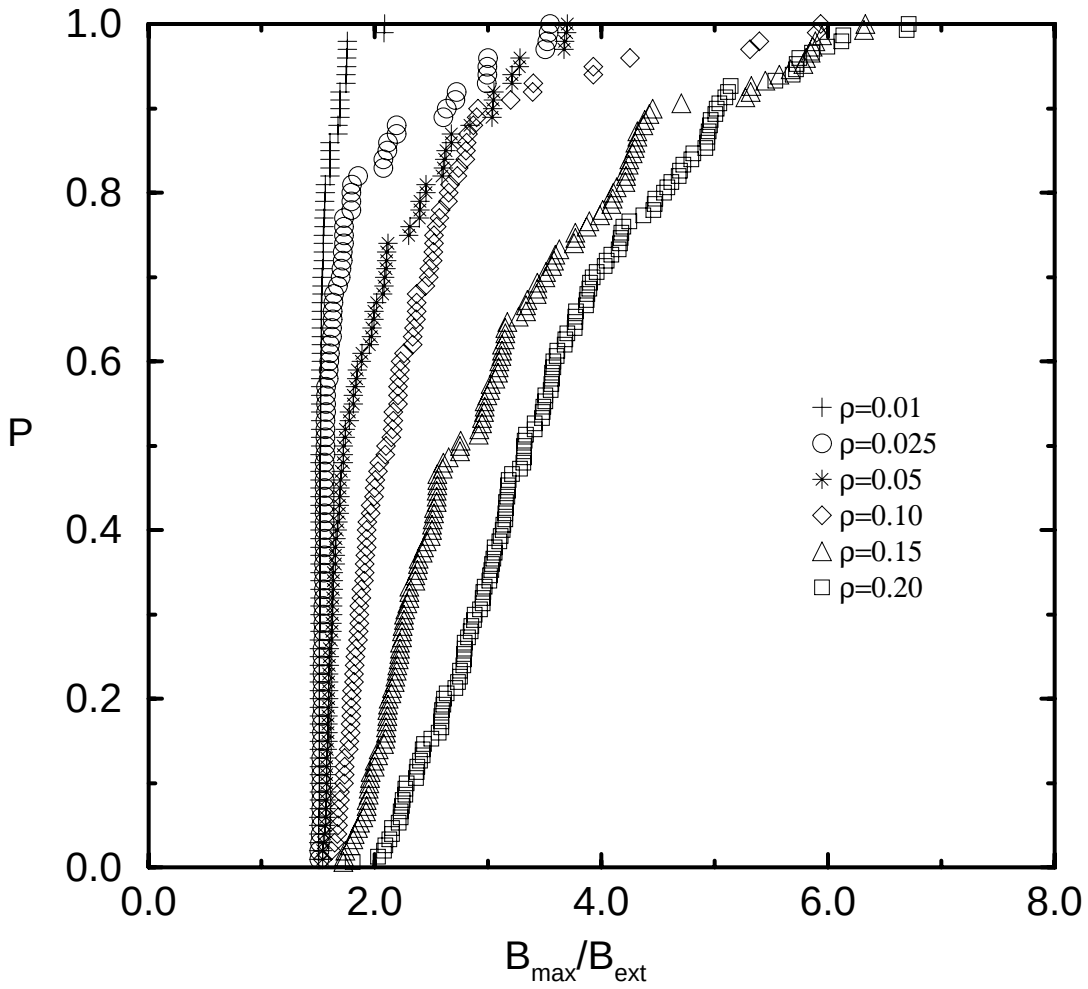

Fig. 4 A. Penaranda et al

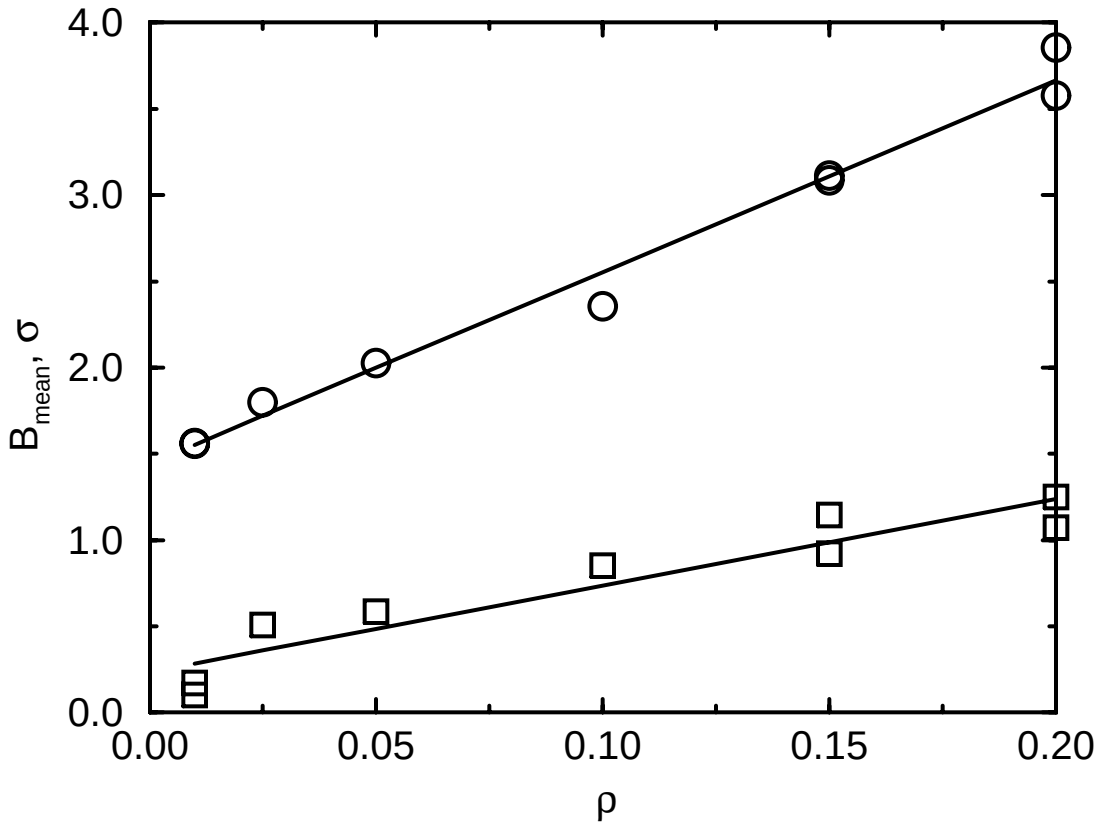

Figure 5 A. Penaranda et al.

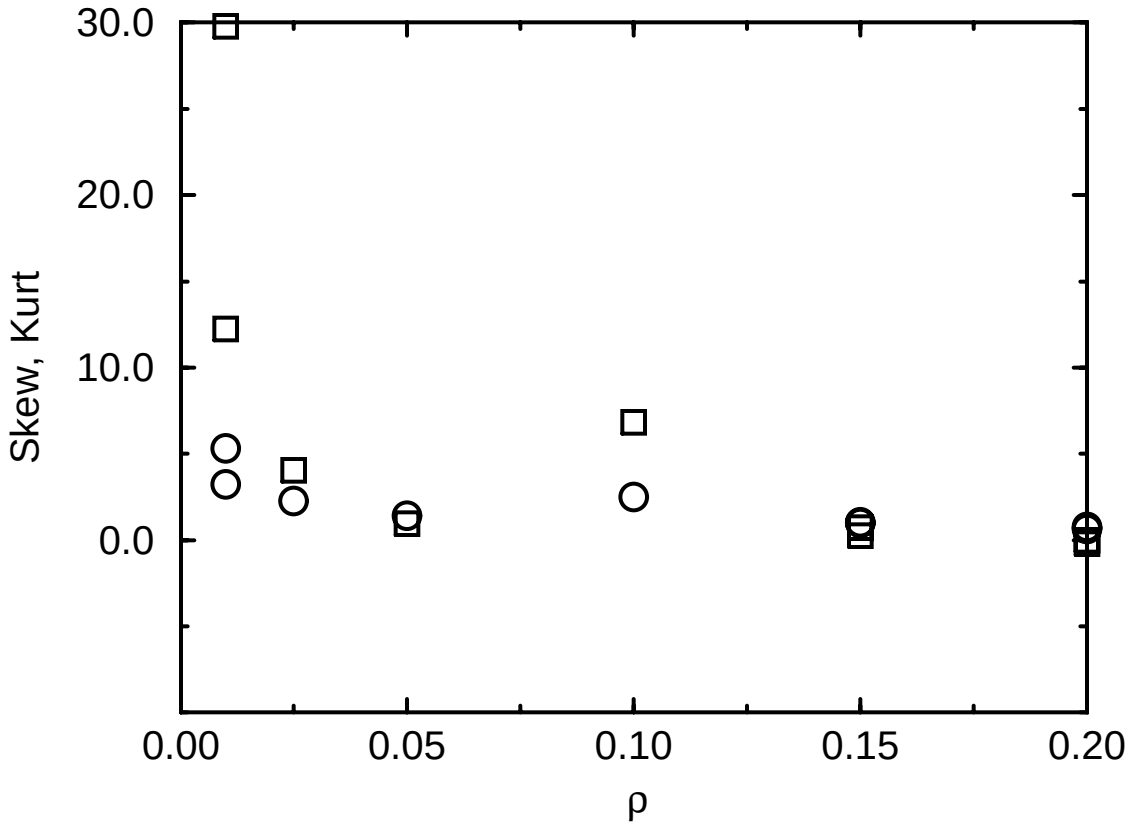

Figure 6 A. Penaranda et al.

Figure 7 A. Penaranda et al.

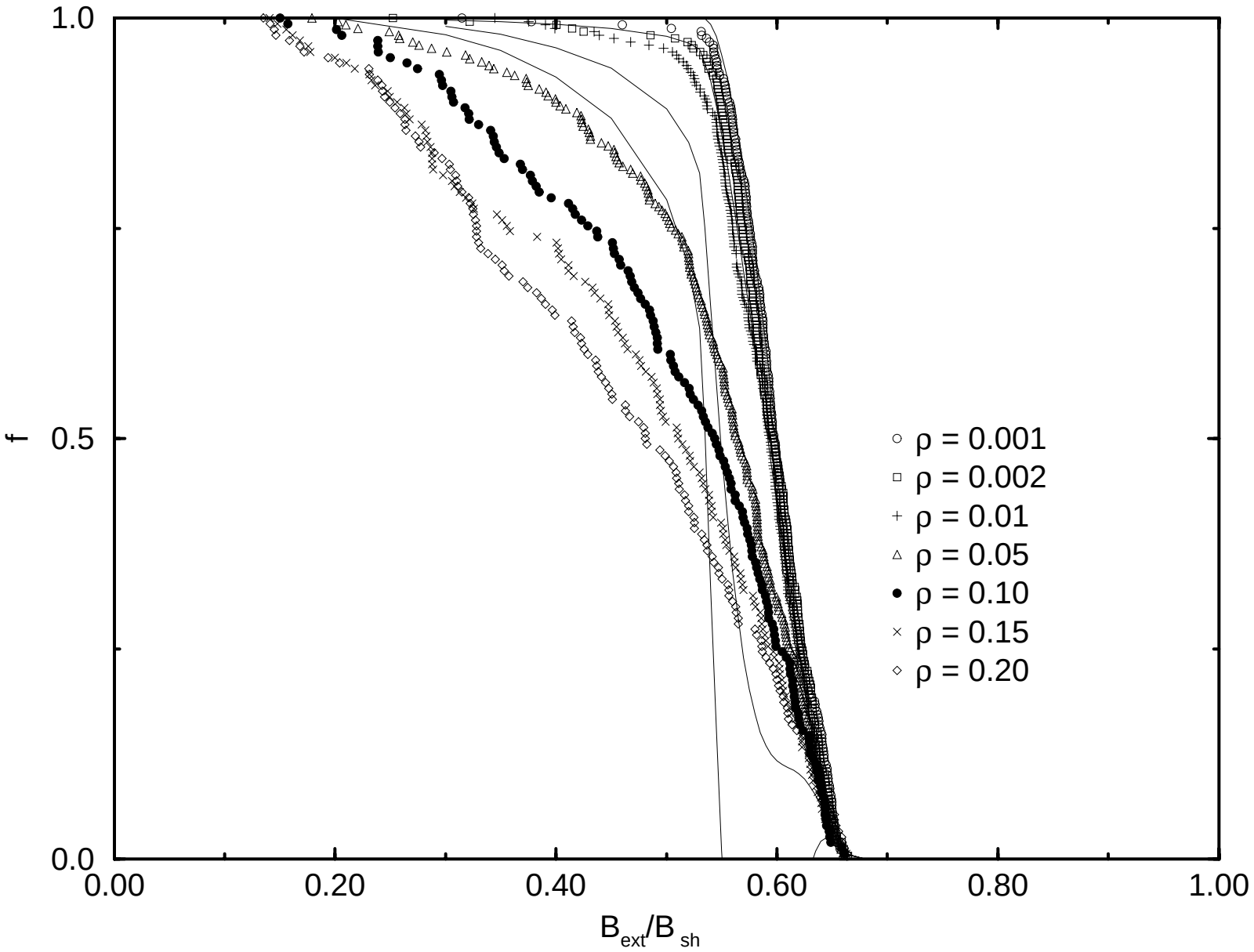

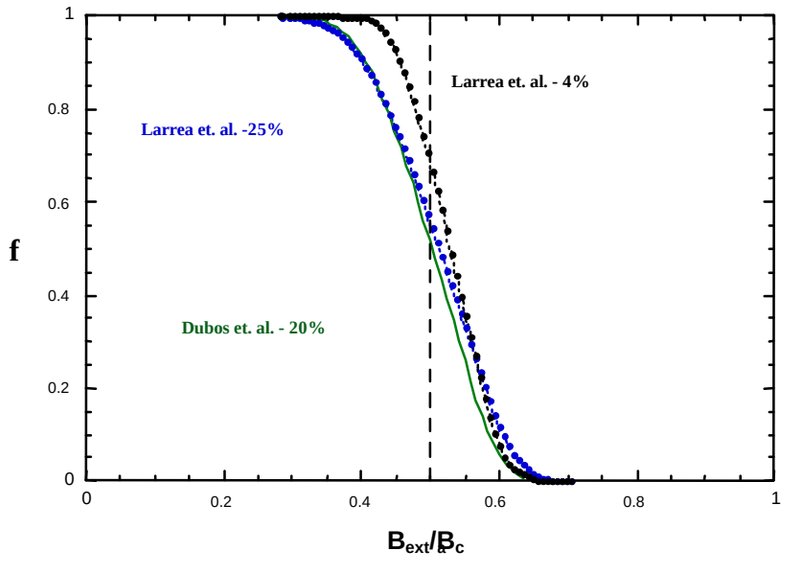

Figure 8 A. Penaranda et al.

Figure 9 A. Penaranda et al.

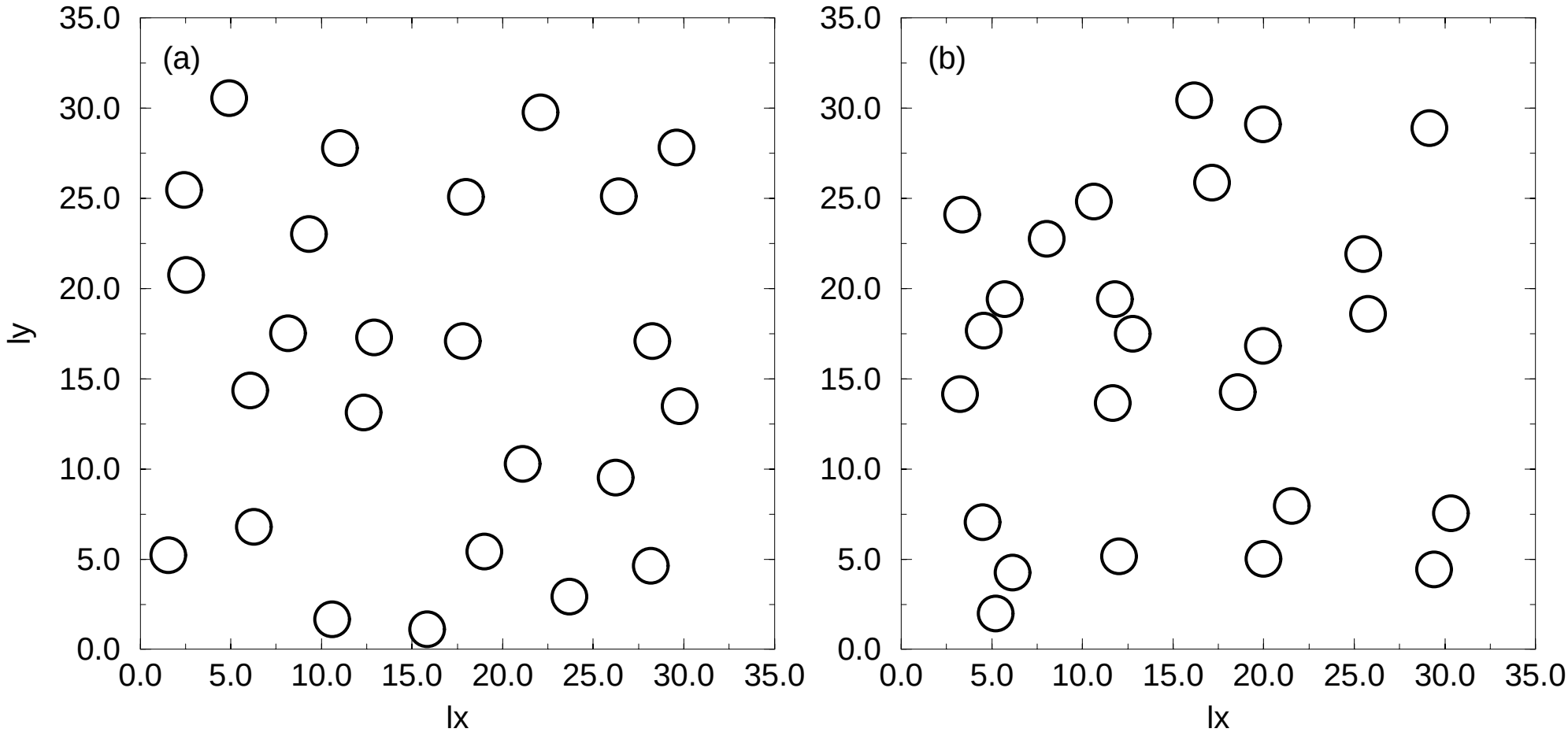

Figure 10 A. Penaranda et al.

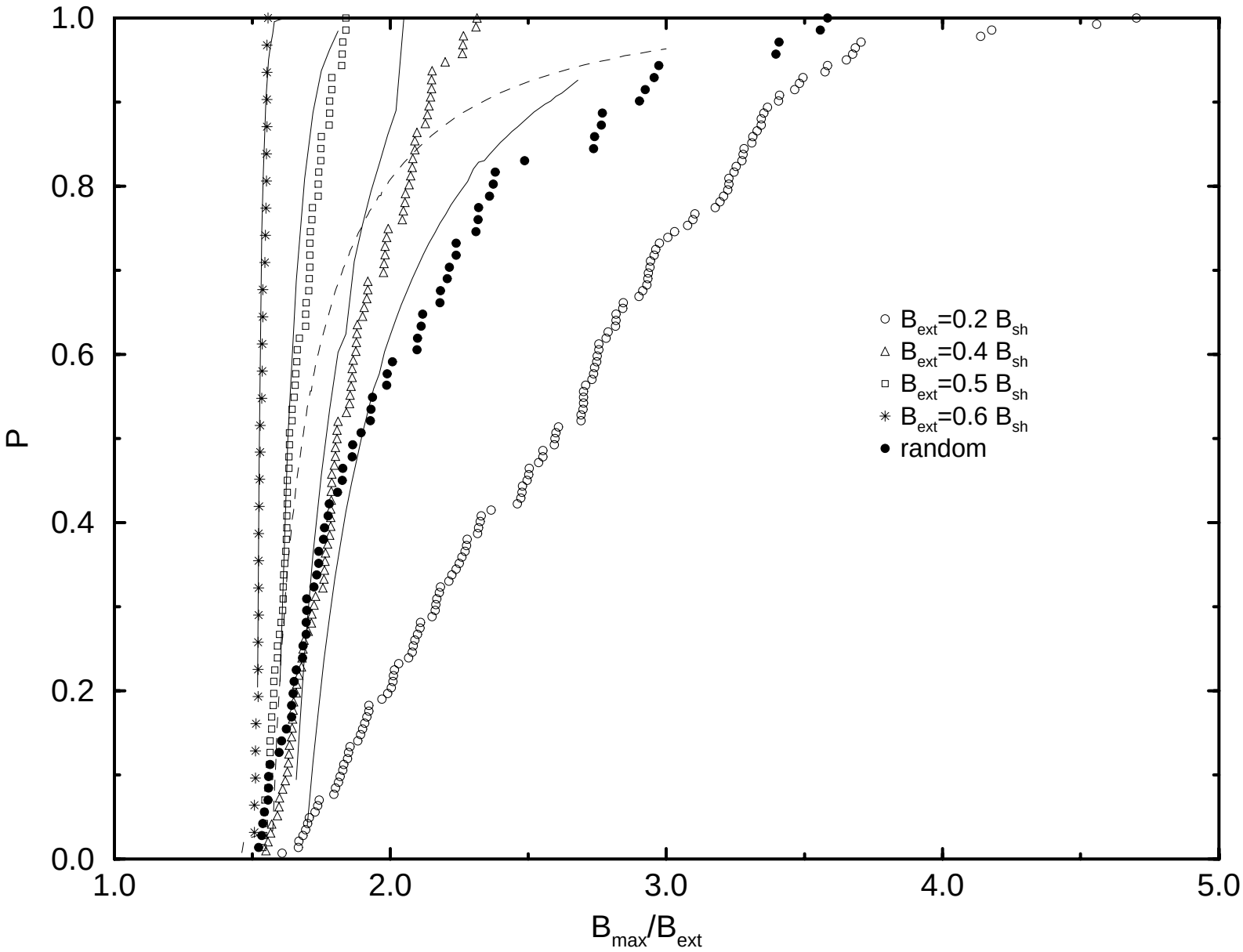

Figure 11 A. Penaranda et al.

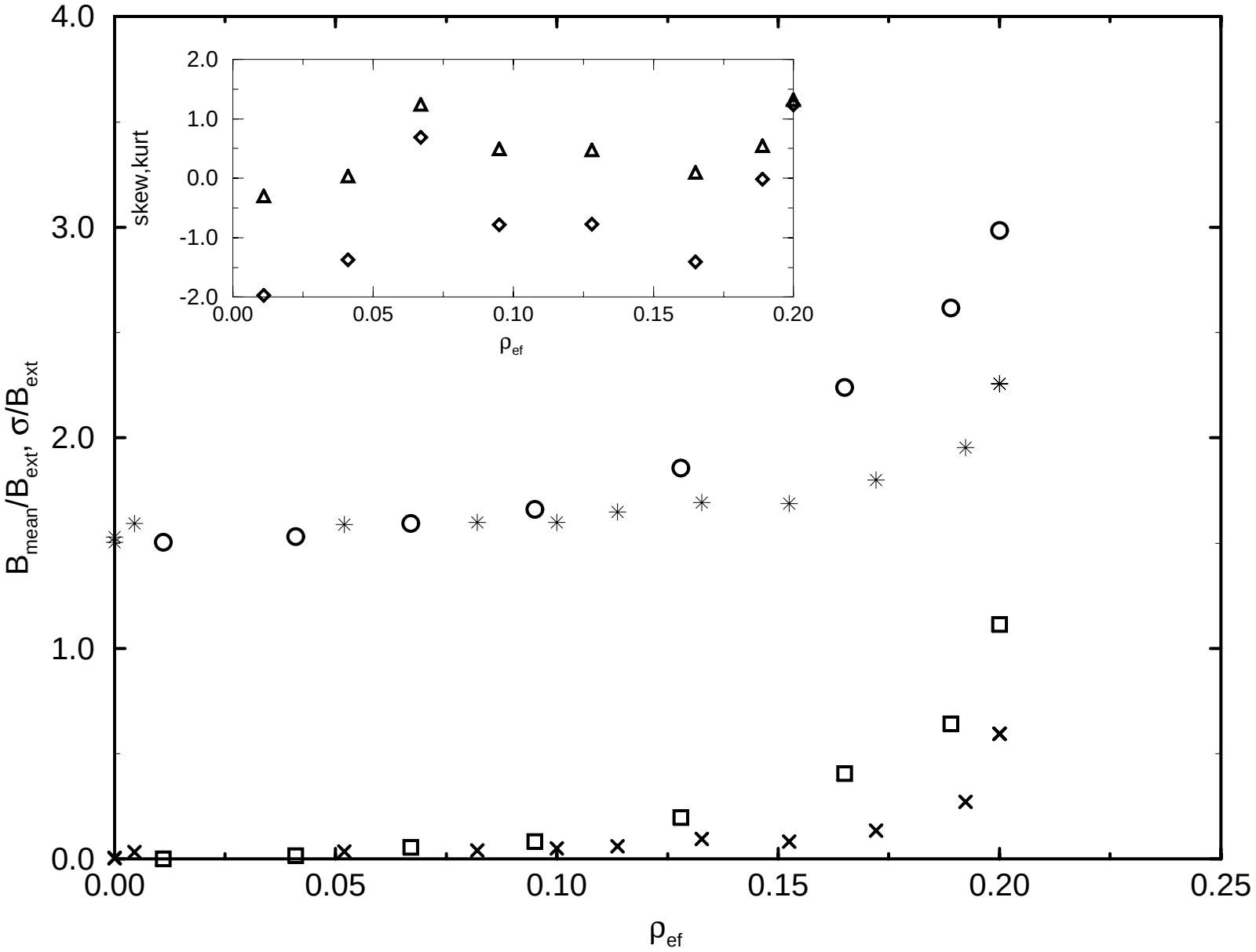

Figure 12 A. Penaranda et al.

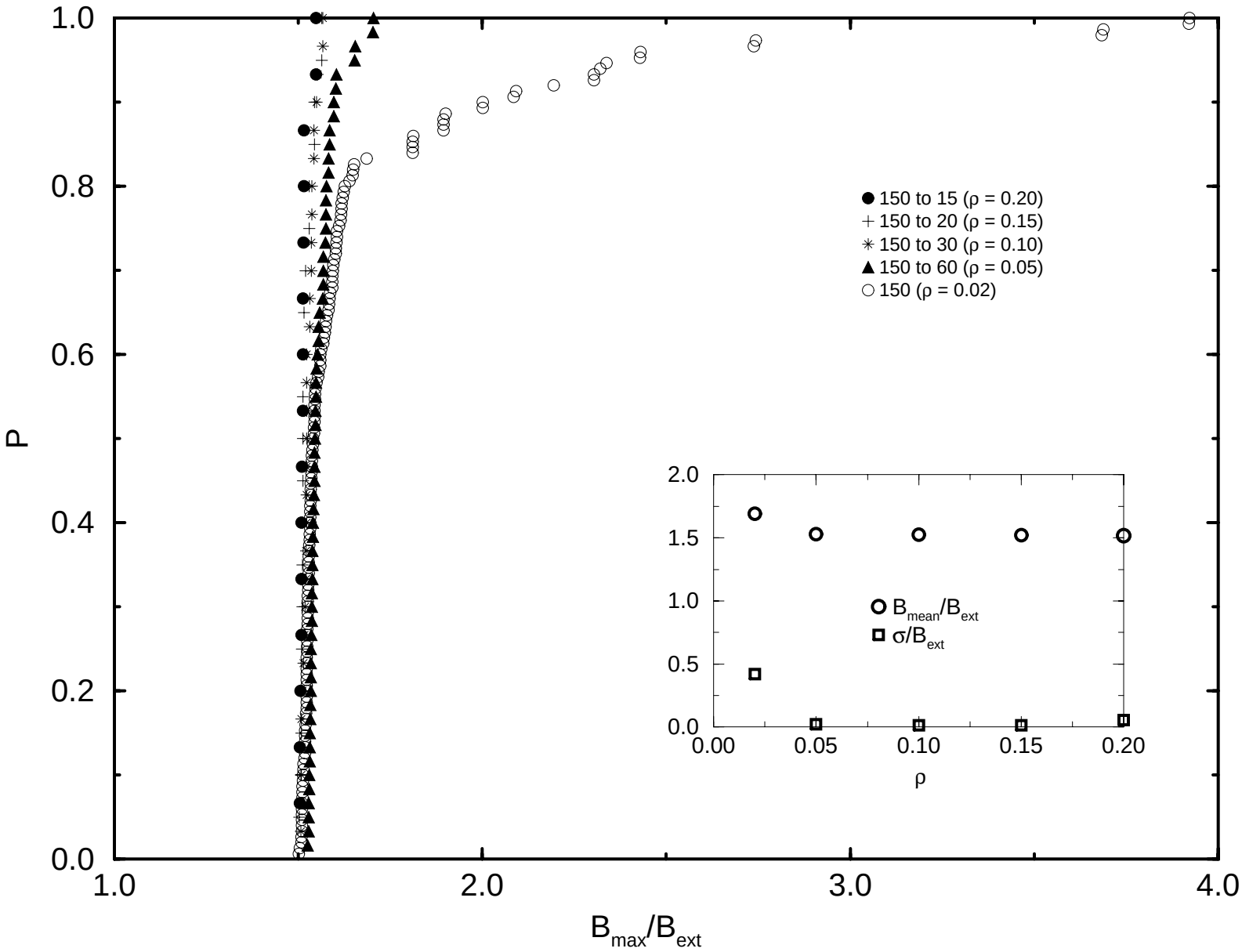

Fifure 13 A. Penaranda et al.

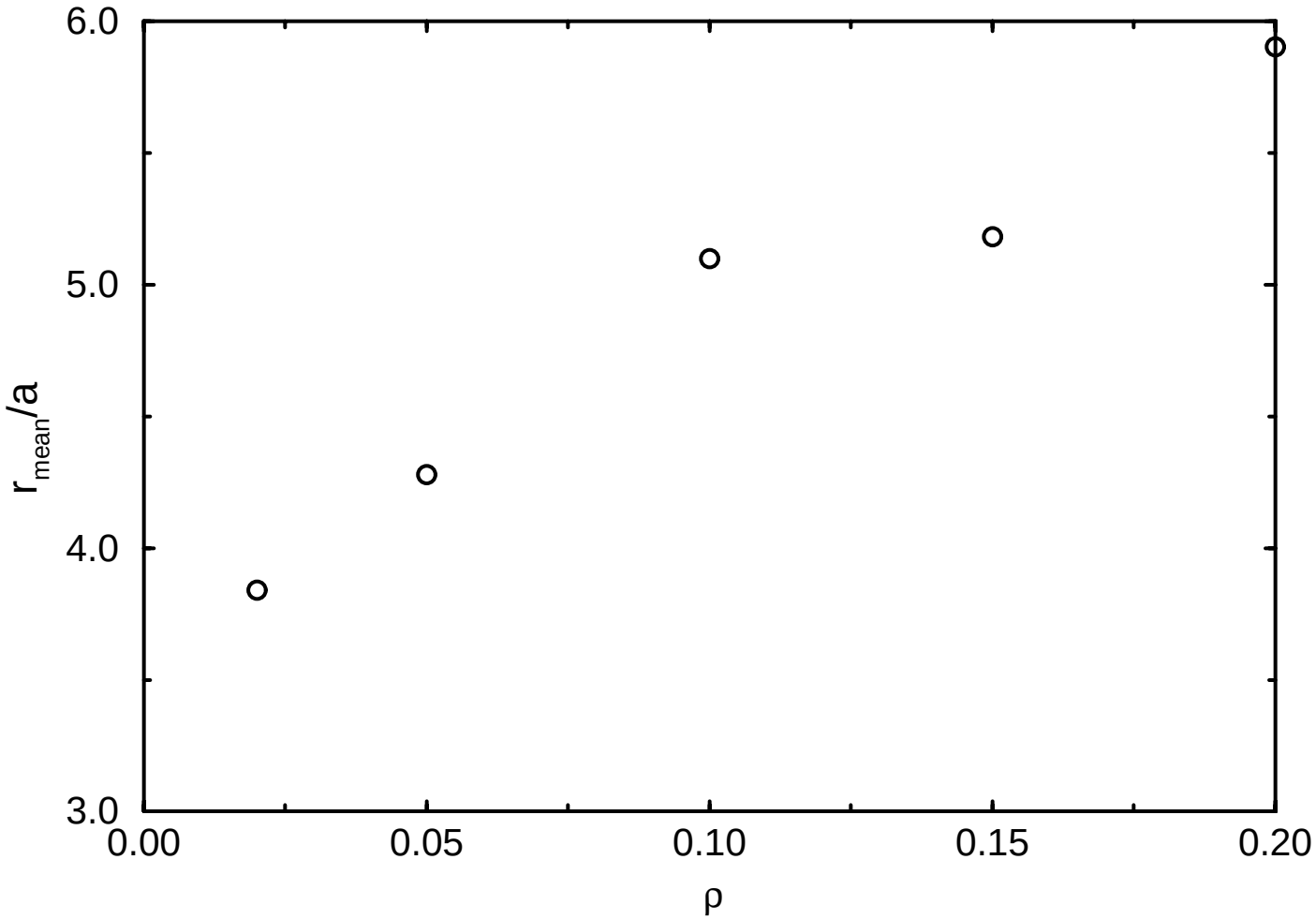

Figure 14 A. Penaranda et al.

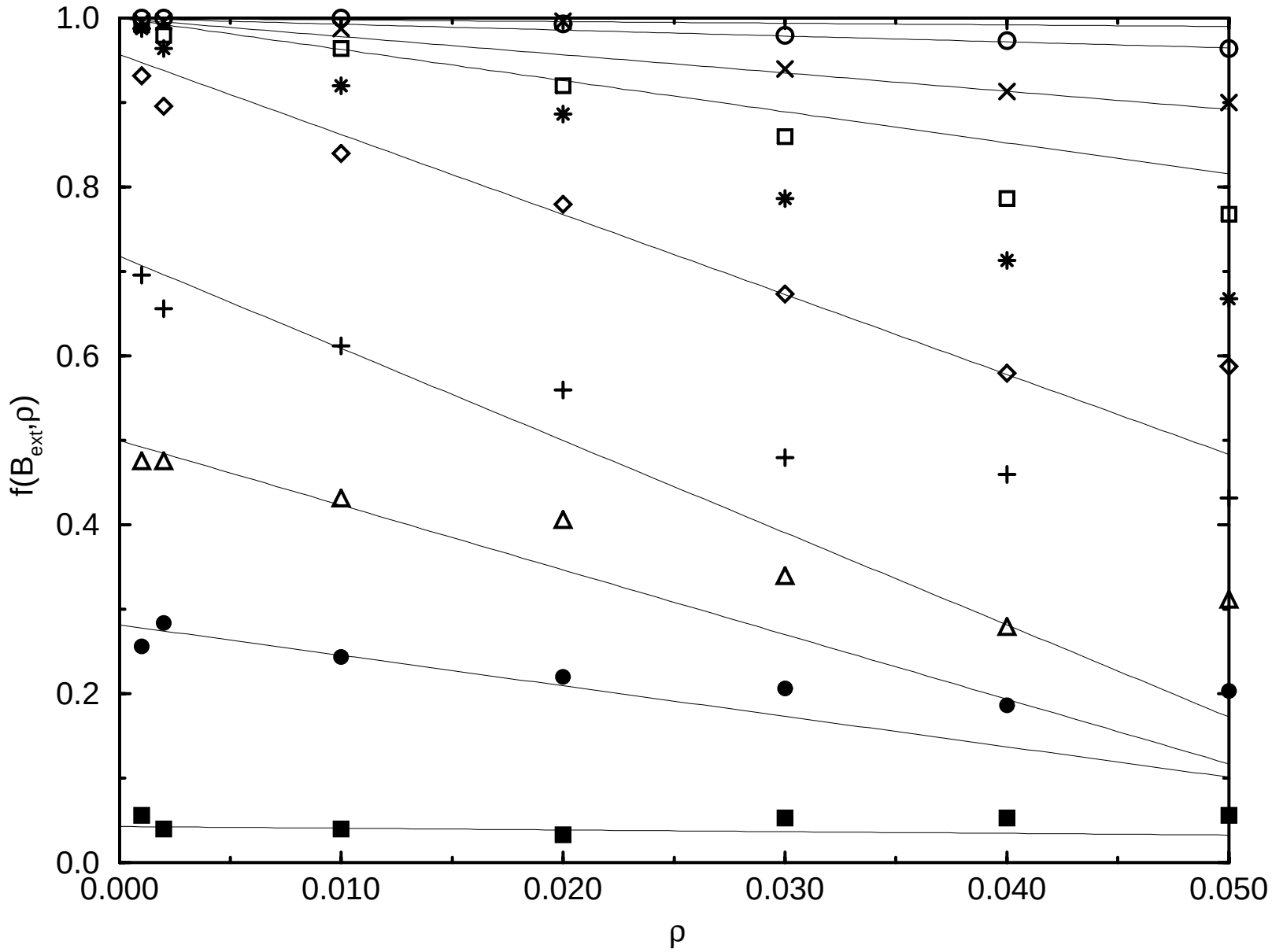

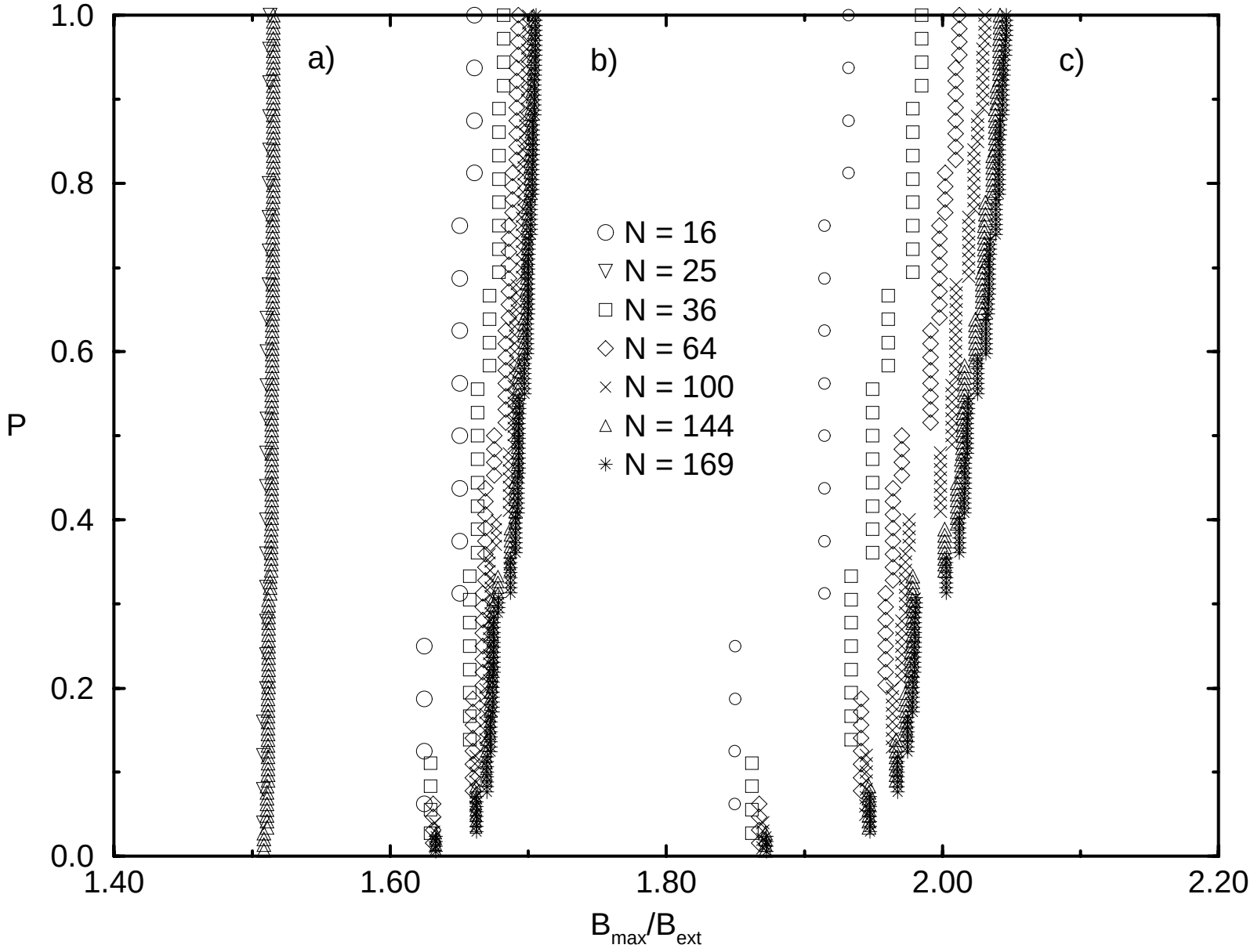

Figure 15 A. Penaranda et al.

Fig. 16 A. Penaranda et al.

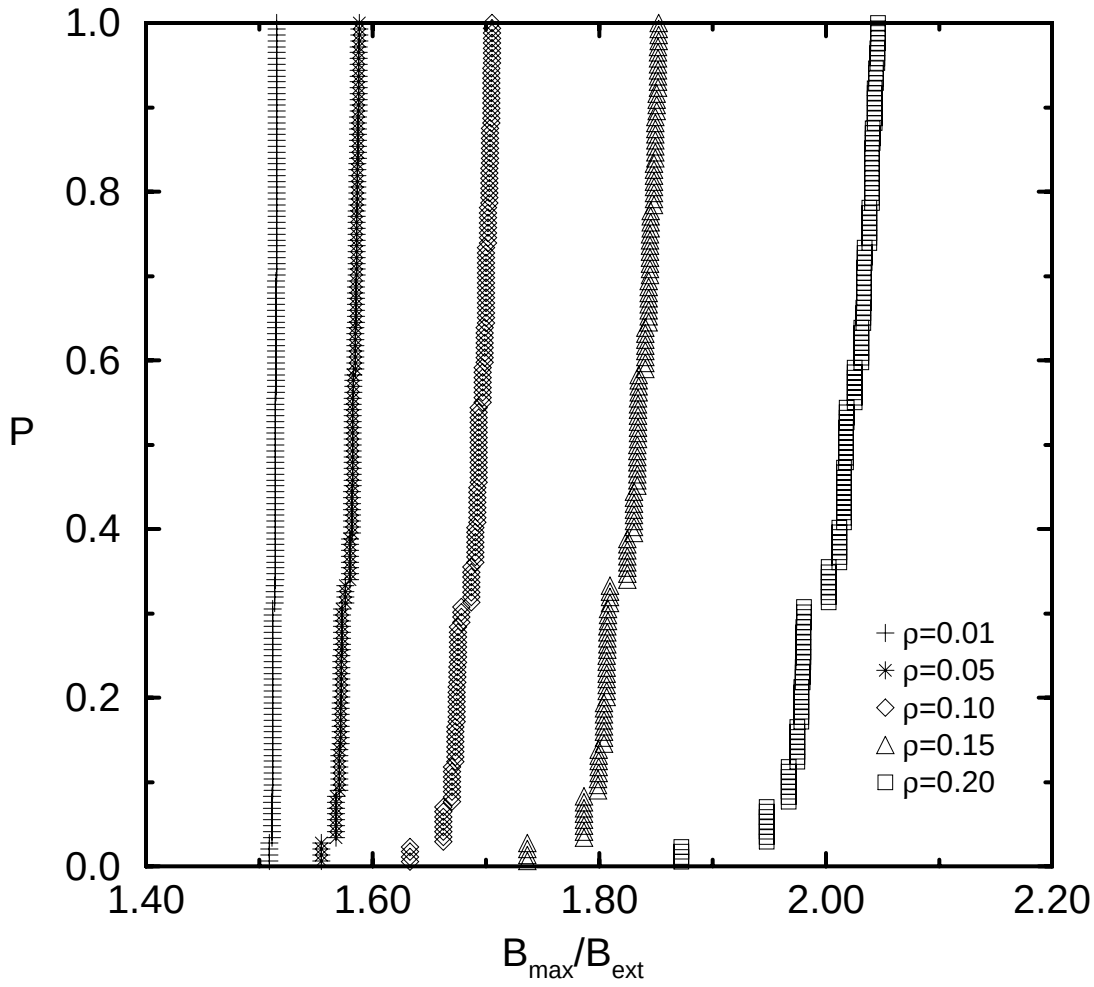

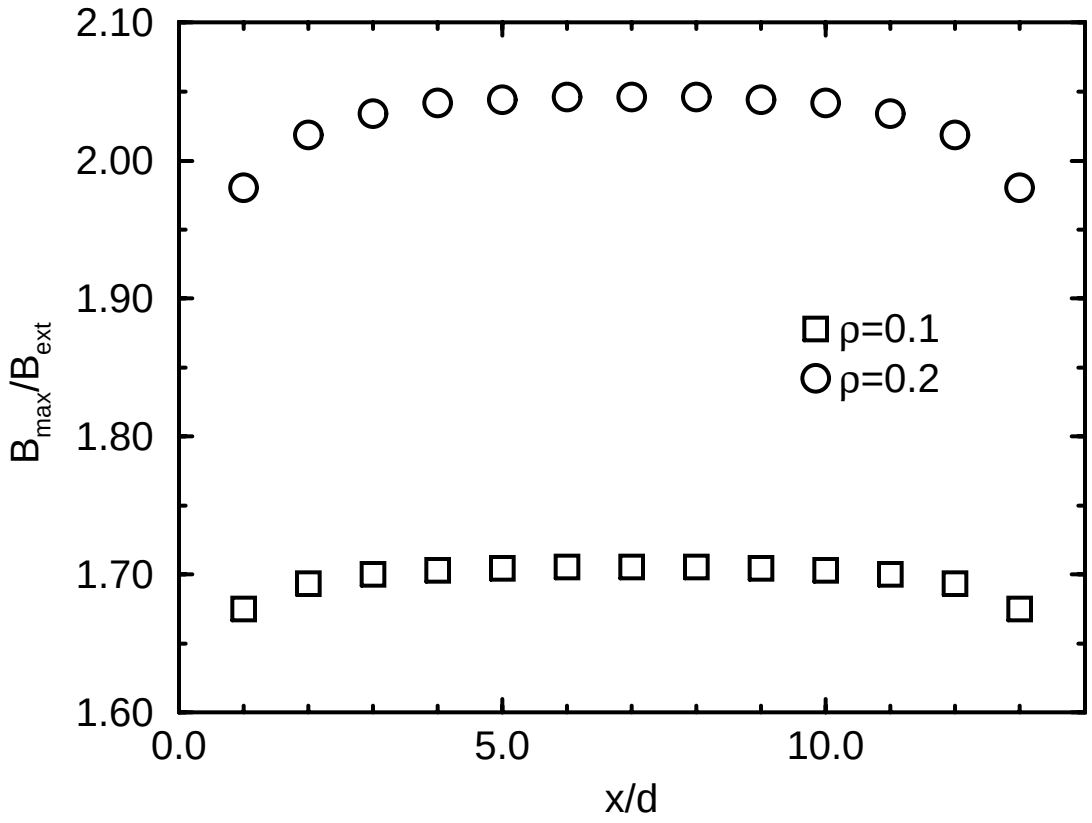

Figure 17 A. Penaranda et al.

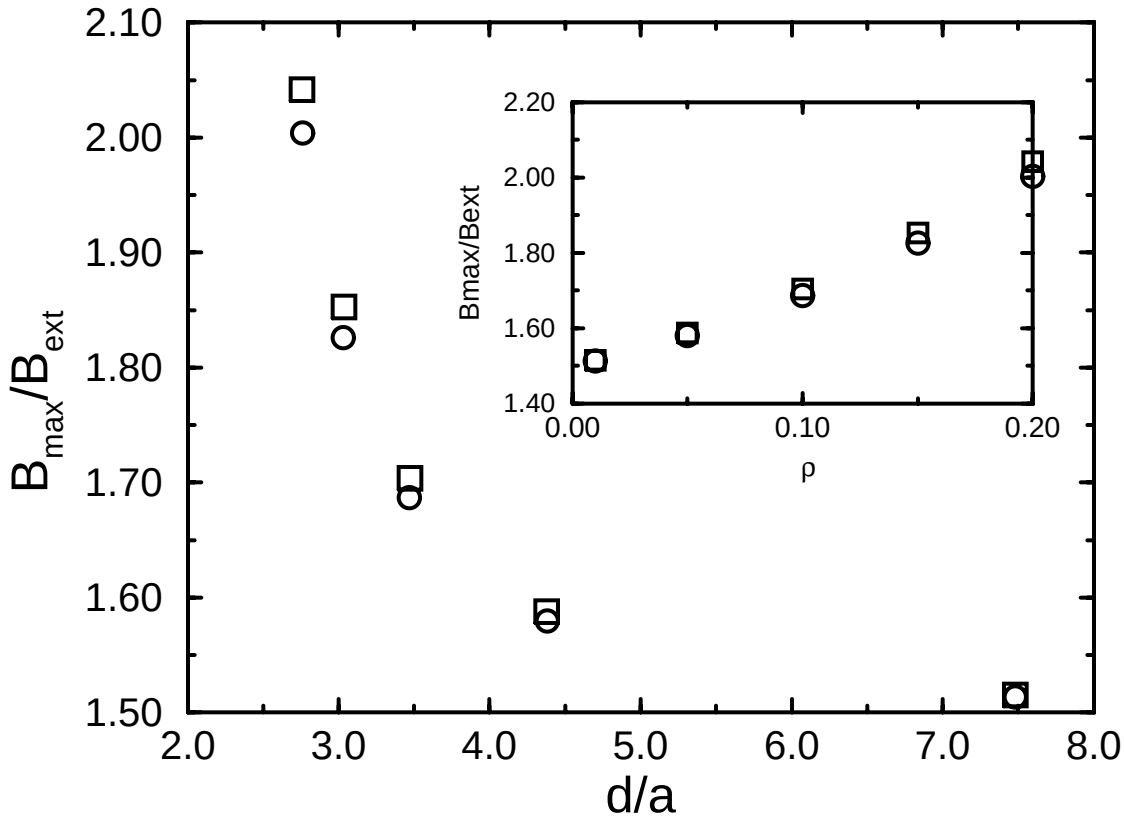

Figure 18 A. Penaranda et al.

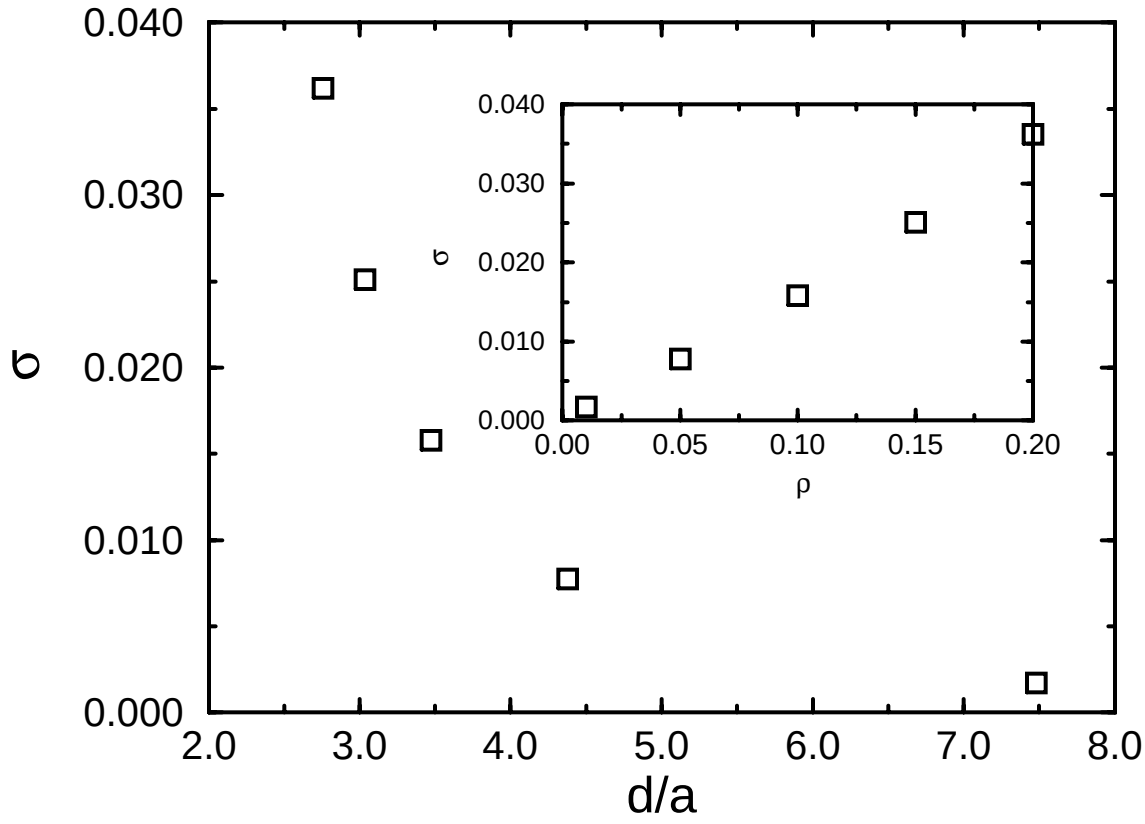

Figure 19 A. Penaranda et al.

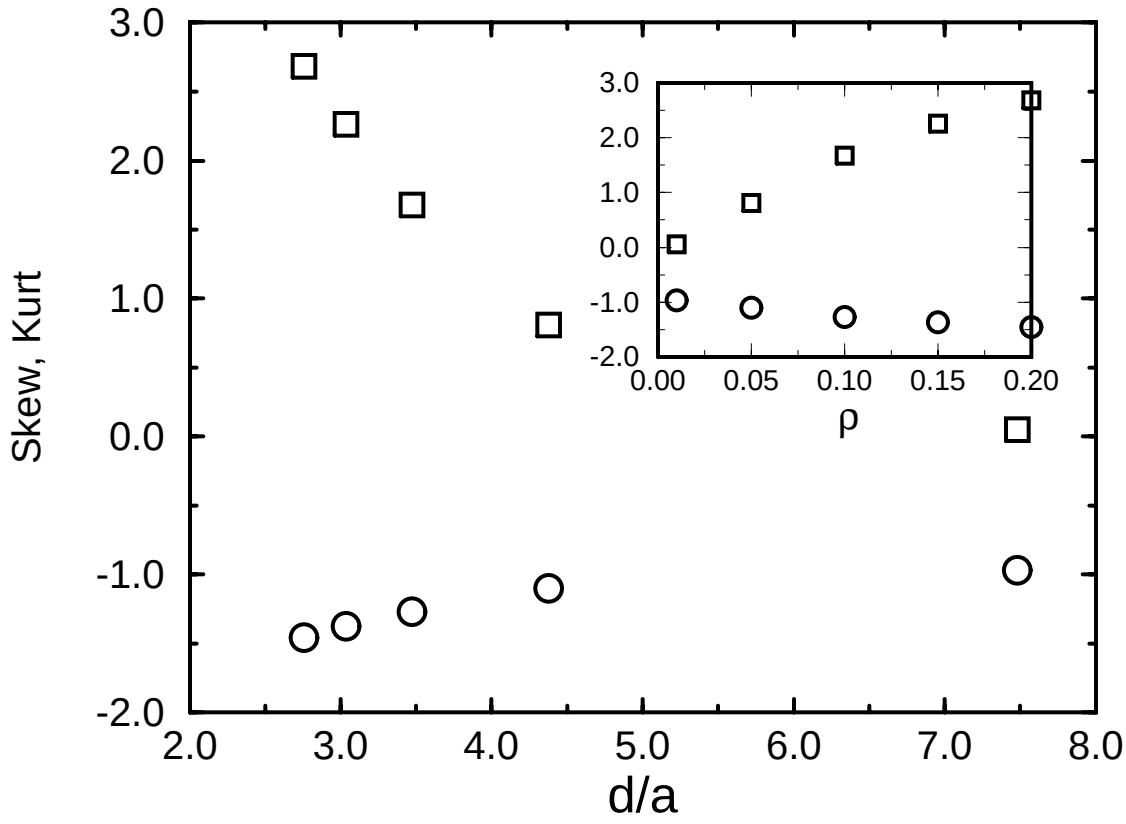

Figure 20 A. Penaranda et al.

Figure 21 A. Penaranda et al.

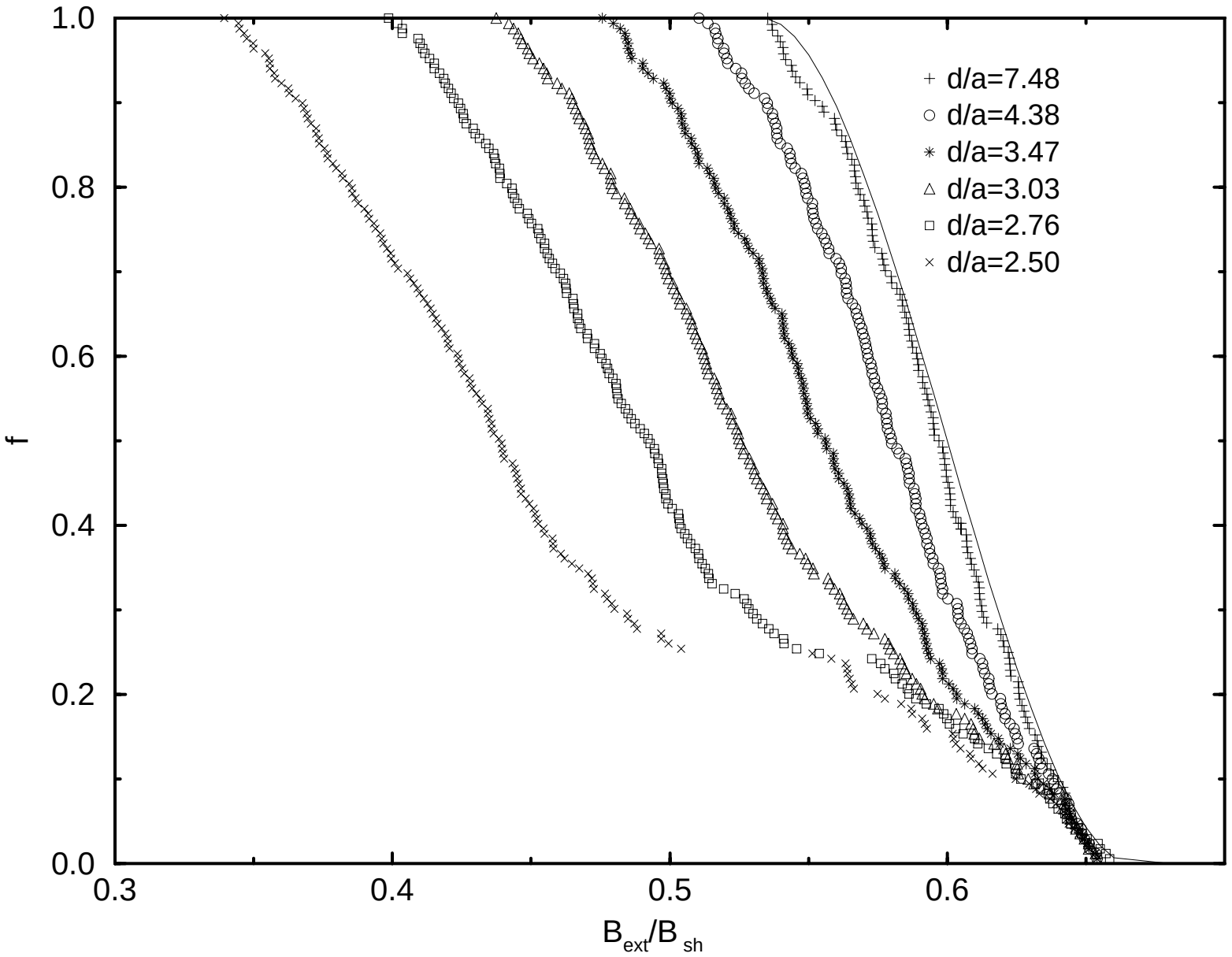

Figure 22 A.Penaranda et al.